ROLE OF MELTING PROCESS AND MELT-ROCK REACTION IN THE FORMATION OF JURASSIC MORB-TYPE BASALTS (ALPINE OPHIOLITES)

Maria Rosaria Renna[a], Riccardo Tribuzio[b,c], Alessio Sanfilippo[b,c], Matthew Thirlwall[d]

[a] Dipartimento di Scienze Matematiche e Informatiche, Scienze Fisiche e Scienze della Terra, Università di Messina, Viale F. Stagno D'Alcontres 31, 98166 Messina, Italy

[b] Dipartimento di Scienze della Terra e dell'Ambiente, Università di Pavia, Via Ferrata 1, 27100 Pavia, Italy

[c] C.N.R. - Istituto di Geoscienze e Georisorse, U. O. di Pavia, Via Ferrata 1, 27100 Pavia, Italy

[d] Department of Earth Sciences, Royal Holloway University of London, Egham TW20 0EX, UK

Corresponding author:

Maria Rosaria Renna

e-mail: mrenna@unime.it

Abstract

This study reports a geochemical investigation of two thick basalt sequences, exposed in the Bracco-Levanto ophiolite (northern Apennine, Italy) and in the Balagne ophiolite (central-northern Corsica, France). These ophiolites are considered to represent an oceanward and a continent-near paleogeographic domain of the Jurassic Liguria-Piedmont basin. Trace elements and Nd isotopic compositions were examined to obtain information about: (i) mantle source and melting process, and (ii) melt-rock reactions during basalt ascent. Whole-rock analyses revealed that the Balagne basalts are slightly enriched in LREE, Nb and Ta with respect to the Bracco-Levanto counterparts. These variations are paralleled by clinopyroxene chemistry. In particular, clinopyroxene from the Balagne basalts has higher Ce_N/Sm_N (0.4-0.3 vs. 0.2) and Zr_N/Y_N (0.9-0.6 vs. 0.4-0.3) than that from the Bracco-Levanto basalts. The basalts from the two ophiolites have homogeneous initial Nd isotopic compositions (initial ε_{Nd} from +8.8 to + 8.6), within typical depleted mantle values, thereby excluding an origin from a lithospheric mantle source. These data also reject the involvement of contaminant crustal material, as associated continent-derived clastic sediments and radiolarian cherts have a highly radiogenic Nd isotopic fingerprint (ε_{Nd} at the time of basalt formation = -5.5 and -5.2, respectively). We propose that the Bracco-Levanto and the Balagne basalts formed by partial melts of a depleted mantle source, likely containing a garnet-bearing enriched component. The decoupling between incompatible elements and Nd isotopic signature can be explained either by different degrees of partial melting of a similar asthenospheric source or reaction of the ascending melts with a lower crustal crystal mush. Both hypotheses are reconcilable with the formation of these two basalt sequences in different domains of a nascent oceanic basin.

Introduction

The chemistry of mid-ocean ridge basalts (MORBs) is conventionally used for obtaining information about composition, temperature and pressure of mantle sources as well as the processes of melting and differentiation that occur between melt generation at depth and eruption on the sea floor. Analysis of basalts within individual ridge segments and/or ocean basin has revealed significant heterogeneity, in terms of major, trace element and radiogenic isotope geochemistry (e.g., Hémond et al. 2006; Stracke et al. 2005; Standish et al. 2008; Waters et al. 2011; O'Neill and Jenner 2012; Wilson et al. 2013). This chemical heterogeneity was mainly attributed to: (1) compositional variations in the mantle source (le Roux et al. 2002; Meyzen et al. 2003), (2) different degree and depth of melting reflecting variations in temperature and pressure of mantle (Klein and Langmuir 1987), (3) different mechanisms of melt aggregation, mixing and fractional crystallization during ascent (Grove et al. 1993), (4) processes of interaction of ascending melts with surrounding rocks within the mantle (e.g., Kelemen et al. 1995; Collier and Kelemen 2010; Paquet et al. 2016) and/or the crust (e.g., Lissenberg et al. 2013), (5) variation of spreading rate (Regelous et al. 2016).

The Jurassic Alpine ophiolites (Fig. 1a) are considered the lithospheric remnants of the Liguria-Piedmont basin (e.g., Vissers et al. 2013). They comprise remnants of oceanic crust associated with continental lithospheric material (e.g., Manatschal and Muntener 2009), and "slow spreading ridge type" lithosphere (e.g., Lagabrielle and Cannat 1990; Sanfilippo and Tribuzio 2011), which were inferred to represent marginal and oceanward domains of the basin, respectively. The ophiolitic bodies exposed along Western Alps, Alpine Corsica and Northern Apennine are characterized by a substrate of serpentinized mantle rocks and gabbroic intrusions discontinuously overlain by basalts, which locally form thick lava sequences typically associated with Middle-Upper Jurassic sediments, mainly polymict breccias and radiolarian cherts (e.g., Principi et al. 2004).

Previous geochemical investigations showed that the incompatible trace element signatures of Jurassic basalts overall range from normal to transitional MORB-like affinity (Venturelli et al. 1981; Vannucci et al. 1993; Rampone et al. 1998; Desmurs et al. 2002). This chemical heterogeneity was interpreted to reflect (i) different degrees of fractional melting of an asthenospheric MORB-type source (Vannucci et al. 1993; Rampone et al. 1998) or (ii) two distinct sources, namely a depleted asthenospheric mantle source for the normal-MORB and an 'enriched' mantle for the transitional-MORB (Desmurs et al. 2002). More recently, the HREE-depleted patterns showed by basalts from External Ligurian (Northern Apennine, Italy) and Alpine Corsica ophiolites, and exemplified by relatively elevated Sm/Yb ratios, were interpreted to reflect an origin by a heterogeneous mantle source containing a garnet-bearing enriched component (Montanini et al. 2008; Saccani et al. 2008).

The present work reports data on two thick basalt sequences exposed in the Balagne ophiolite (central-northern Corsica, France) and Bracco-Levanto ophiolite (Northern Apennine, eastern Liguria, Italy). The Balagne basalt sequence locally includes layers of quartzo-feldspathic clastic sediments, thereby documenting that the Balagne ophiolite was originally adjacent to a continental margin (Durand-Delga et al. 1997, Marroni and Pandolfi 2007; Renna et al. 2017). On the basis of incompatible trace element compositions, the Balagne basalts were proposed to have transitional-MORB affinity (e.g., Venturelli et al. 1981), which was attributed to either crustal contamination (Durand-Delga et al. 1997) or a contribution from a lithospheric mantle source (Saccani et al. 2008). The Bracco-Levanto ophiolite does not include continental material and is considered to be formed in an oceanward domain of the Jurassic basin (e.g., Tribuzio et al. 2016). Previous geochemical studies of basalts collected at the top of the Bracco-Levanto ophiolite showed that they have a MORB-type elemental and isotopic signature (Rampone et al. 1998; Barry et al. 2016).

In the present study, whole-rock and clinopyroxene major and trace element analyses, coupled with Nd isotope whole-rock determinations were examined to obtain information about the mantle source materials and to shed light about the processes responsible for the formation of basalts with

92 heterogeneous incompatible elements signatures. We will present evidence for an origin of the
93 basalts from a depleted mantle source. We discuss two different petrogenetic scenarios where
94 different degrees of partial melting and/or reaction within the lower oceanic crust produced basalts
95 characterized by similar Nd isotope compositions but slightly different incompatible element
96 signatures.

97 ## Geological framework

98 ### Balagne ophiolite

99 The Balagne ophiolite is located at the top of Alpine Corsica stack and is unaffected by the
100 high pressure/low temperature metamorphism typical of tectonic units from the Schistes Lustrés
101 units (e.g., Molli and Malavieille 2011). The ophiolite (Fig. 1) is mainly made up of pillow basalts
102 locally interlayered with levels of massive basalts previously interpreted as dolerite layers (Baud
103 1975; Gruppo di Lavoro sulle Ofioliti Mediterranee 1977; Durand-Delga 1984). The massive
104 basalts layers are up to 10 metres thick and typically occur in the upper sector of the basalt
105 sequence. Each layer shows grain size decrease from the center to the margins of the layer. In
106 addition, the contact between the different layers is characterized by the occurrence of vesicles
107 typically filled with calcite. Fine-grained pelagic sediments are also locally intercalated between
108 each basalt layer. The pillow basalts are primarily associated with: (i) polymict breccias containing
109 gabbro and basalt clasts, which mostly occur at the stratigraphic base of the ophiolite, and (ii)
110 quartzo-feldspathic clastic sediments mostly derived from Permian continental material (Durand-
111 Delga et al. 2001; Rossi et al. 2002; Marroni and Pandolfi 2003; Renna et al. 2017). The pelagic
112 sediments capping the basalts are Middle-Upper Jurassic radiolarian cherts grading upward into
113 Cretaceous Calpionella limestones and Palombini shales (Chiari et al. 2000; Bill et al. 2001;
114 Peybernés et al. 2001; Danelian et al. 2008). The Calpionella limestones are locally overlain by a
115 sequence of massive calcarenite-breccia, which contains fragments of volcano-clastic material,
116 granites and metamorphic rocks interpreted to derive from the Corsica batholith (Durand-Delga et

al. 1997). The thickness of the entire succession was estimated to be ~500 m (Marroni and Pandolfi 2003).

The Balagne ophiolite also includes a ~100 m thick tectonic slice composed of an intrusive sequence (gabbronorites, oxide-rich gabbros and albitites) topped by basalts (Fig. 1). U-Pb zircon geochronology dated the formation of this intrusive sequence at 159 ± 3 Ma (Renna et al. 2017), which is contemporaneous with the formation of the ophiolitic gabbros from the adjacent Schistes Lustrés units (Li et al. 2015). A slightly older U-Pb zircon age of 169 ± 3 Ma was obtained for a leucocratic felsic dyke crosscutting an oxide-rich gabbro clast in the polymict breccias (Rossi et al. 2002). It is worth noting that the U-Pb zircon ages of 159 ± 3 Ma and of 169 ± 3 Ma are associated with a relatively high MSWD (6.3, n = 18 and 8.4, n = 11, respectively), thereby suggesting that further geochronological investigations are needed to assess a precise and accurate age of the lower crust formation for the Balagne ophiolite (see further discussion in Renna et al. 2017). For the scope of this study, we will consider an average age of 164 Ma for the basalts sampled in the Balagne ophiolite.

Bracco-Levanto ophiolite

The Bracco Levanto ophiolite consists of a basement made up of gabbros intruding depleted mantle peridotites, and a heterogeneous basalt-sedimentary sequence (Cortesogno et al. 1987; Principi et al. 2004). The mantle sequences are formed by spinel to plagioclase harzburgites to clinopyroxene-rich lherzolite, locally including replacive, dunite bodies (Sanfilippo et al. 2014). The stratigraphic top of the mantle sequences is characterized by faulted serpentinites rich in calcite-veins and hematite, which developed in conjunction with seafloor exposure (Treves and Harper 1994; Schwarzenbach et al. 2012). The gabbroic sequences formed at 162-161 Ma (Tribuzio et al. 2016) and mainly consist of olivine gabbro to clinopyroxene-rich gabbro with a MOR-type geochemical signature (Rampone et al. 1998; Sanfilippo and Tribuzio 2011). They include olivine-rich troctolite bodies and mantle peridotite slivers at different stratigraphic levels (Renna and

142 Tribuzio 2011; Renna et al. 2016). The gabbroic bodies include granulite facies ductile shear zones
143 that are locally crosscut at a high angle by hornblende veins documenting migration of seawater-
144 derived fluids (Tribuzio et al. 1995; 2014).

145 The basalt-sedimentary sequence typically shows interlayering among basalts, polymict
146 breccias and Middle to Upper Jurassic radiolarian cherts (Abbate et al. 1980). The thickness of the
147 basalt-sedimentary sequence is however in places reduced to a few meters or even absent, with the
148 gabbro-peridotite basement directly overlain by Cretaceous shaly pelagites (Cortesogno et al. 1987).
149 The rocks considered in the present study were collected in the Bonassola area, where a thick
150 basalt-sedimentary sequence is exposed (Fig. 1, see also Principi et al. 2004). The basalt-
151 sedimentary succession here shows at the base a thin level of serpentinitic breccia, which
152 unconformably overlies the faulted serpentinite basement and is locally associated with Middle
153 Jurassic radiolarian cherts (Chiari et al. 2000). The serpentinitic breccia is covered by a layer (up to
154 400 m thick) mainly consisting of massive basalts layers, which show grain size decrease from the
155 center to the margins of the layer and are interlayered with up to m-scale thick levels made up of
156 basalt breccias and radiolarian cherts. The basalt-sedimentary layer is covered by a polymict breccia
157 containing clasts of gabbros, basalts and serpentinites. In the more western sector, this polymict
158 breccia is overlain by conspicuous pillow lava (up to 200 m thick), in turn capped by pelagic
159 deposits represented by radiolarian cherts grading upward to Cretaceous Palombini shales.

160 ## Selected samples

161 We selected eight samples from the massive basalt layers, in particular four samples from
162 Balagne (N1, N10, N21, RF2) and four from Bracco-Levanto (ROS12, ROS10, ROS6, ROS9)
163 ophiolites. They were collected in the medium-grained centers of the layers and at different
164 stratigraphic positions, from the top to the bottom of the main basalt-sedimentary succession (Fig.
165 1, Table 1). The selected samples display sub-ophitic texture (Fig. 2a). They mostly consist of
166 euhedral to subhedral plagioclase (60-50 vol%) and subhedral to anhedral clinopyroxene (45-30

167 vol%). The latter has concentric or patchy optical zoning, with pale brown cores and brown rims.
168 All samples contain accessory to minor amount of skeletal Fe-Ti oxides (up to 5 vol%) and
169 accessory acicular apatite, which is commonly hosted by plagioclase and clinopyroxene. Two
170 samples (ROS6 and ROS10) from the Bracco-Levanto succession contain minor amounts of
171 anhedral quartz (5 vol%) generally associated with/or rimmed by chlorite (Fig. 2b). The quartz-
172 chlorite association commonly hosts prismatic to acicular apatite and locally includes epidote ± Fe-
173 Ti oxides ± actinolite. In all samples, plagioclase is replaced by fine-grained aggregates of albite ±
174 epidote ± chlorite and clinopyroxene by chlorite ± actinolite, Fe-Ti oxides is locally rimmed by
175 leucoxene.

176 Within the Balagne basalt-sedimentary succession, we also considered a sample of quartzo-
177 feldspathic breccia (PC11) and a sample of carbonate-rich quartzitic sandstone (PP1) from two
178 levels of quartzo-feldspathic clastic sediments (Fig. 1). These samples were described by Renna et
179 al. (2017). Sample PC11 consists of a microcrystalline siliceous matrix including (i) medium to
180 coarse-grained clasts of locally prismatic feldspars, (ii) quartz mainly with engulfed shape or as
181 irregular grains locally partially recrystallized to fine-grained aggregates, (iii) rare fine-grained dark
182 mica replaced by fine-grained aggregates of chlorite + white mica + titanite. Quartzitic sandstone
183 PP1 is made up of a calcite-rich microcrystalline matrix including fine-grained clasts of (i) quartz as
184 engulfed single crystal or polygonal aggregates, (ii) feldspars and (iii) calcite as irregular grains or
185 shell fragments of crinoids and foraminifera (see also Rossi et al. 2001).

186 Two samples (ROS22 and ROS25) of radiolarian cherts from a meter-scale thick layer included
187 within the massive basalt succession of Bracco-Levanto were also selected (Fig. 1). The samples are
188 fine-grained and dark red in color and mainly consist of quartz, minor chlorite and accessory
189 hematite. Radiolarians constitute 10 vol% and 40 vol% of sample ROS22 and ROS25, respectively.
190 Sample ROS25 also contains accessory amounts of calcic amphibole.

Analytical technique

Whole rock major and trace element analyses of the selected samples (Table 2) were carried out at Activation Laboratories LTD (Ancaster, Ontario) by inductively coupled plasma (ICP) optical emission spectroscopy and ICP mass spectrometry (method 4Lithores - Lithium Metaborate/Tetraborate Fusion - ICP and ICP/MS). Three blanks and five controls (three before sample group and two after) were analyzed per group of samples. Detection limits and values for standard material during the analyses are compiled in a table uploaded as supplementary material. Precision and accuracy of trace element analyses are assessed to be within 10%.

Whole rock Nd isotopic ratios and Sm-Nd concentrations of selected samples (Table 3) were determined at the Department of Geology, Royal Holloway, University of London on a multi-collector VG354 mass spectrometer using multidynamic techniques procedures and normalization described in Thirlwall (1991a,b). All errors are 2SE and relate to the last significant digits. The whole rock powders were leached for 1 h in hot 6 M HCl. Nd were separated for isotope analyses using conventional ion exchange technique after dissolution in Savillex beakers. The $^{143}Nd/^{144}Nd$ value of Aldrich laboratory standard on the day of analyses was 0.511404 (2SD = 0.000004, n = 5), within error of the long-term Aldrich laboratory mean of 0.511405 (2SD = 0.000006, n = 117). Daily variations in $^{143}Nd/^{144}Nd$ ratios were normalized to $^{143}Nd/^{144}Nd = 0.511409$. Mass bias corrections were made using $^{146}Nd/^{144}Nd = 0.7219$.

The pale brown cores of clinopyroxene were analysed for major and trace element concentrations. Major element analyses (Table 4) were carried out at the Dipartimento di Scienze della Terra, Università di Milano with a JEOL 8200 Super Probe, in wavelength-dispersive mode. Operating conditions were 15 kV accelerating voltage, 15 nA beam current and a counting time of 30 s on the peaks and 10 s on the backgrounds. Natural silicates were used as standards.

Trace element analyses of clinopyroxene cores were carried out using laser ablation inductively coupled plasma spectrometry at C.N.R. – Istituto di Geoscienze e Georisorse of Pavia (Table 5).

The laser probe consisted of a Q-switched Nd:YAG laser, model Quantel (Brilliant), whose fundamental emission in the near-IR region (1064 nm) was converted into 213 nm wavelength using three harmonic generators (Jeffries et al. 1998). Spot diameter was typically 40 μm. The ablated material was analyzed by using an Elan DRC-e quadrupole mass spectrometer. Helium was utilized as carrier gas and mixed with Ar downstream of the ablation cell. NIST SRM 610 was utilized as external standard. The CaO content determined by electron microprobe was used as internal standard, scaled on the 44Ca+ signal. Precision and accuracy were assessed from repeated analyses of the BCR2-g standard and resulted usually better than 10% at ppm concentration level. Detection limits were typically in the range of 1.0–0.5 ppm for Cr and Ti, 0.5–0.1 ppm for Sc, 100–10 ppb for Sr, Zr, Ba, Rb, V and Gd, 10–1 ppb for Y, Nb, REE, Hf and Ta.

Whole-rock geochemistry

Basalts

The selected samples from the massive layers of the Balagne and Bracco-Levanto ophiolites fall in the trachybasalt and in the basalt field, respectively, of the total alkali versus silica diagram (TAS, Le Maitre 1989). They will be hereafter referred to as basalts.

Balagne basalts have Mg# [molar $MgO/(MgO+FeO_t) \times 100$] and Al_2O_3 contents varying from 63.3 to 36.6 and from 16.4 to 13.4 wt%, and relatively high TiO_2 contents (3.2-1.5 wt%). The Mg#, Al_2O_3 and TiO_2 values of selected Bracco-Levanto basalts largely overlap those of Balagne basalts (64.5 – 44.5, 17.3 – 12.8 wt% and 2.9 – 1.1 wt%). Both Balagne and Bracco-Levanto basalts show TiO_2 increase with decreasing Mg# (Fig. 3). Balagne basalts have slightly lower CaO than Bracco-Levanto basalts (7.1 - 6.4 wt% vs. 9.5 – 8.9 wt%). The concentrations of Cr and Ni are relatively low (up to 130 ppm and up to 100 ppm, for Balagne basalts, up to 220 ppm and up to 150 ppm for Bracco-Levanto basalts). Balagne and Bracco-Levanto basalts show similar ranges of V contents (351 – 184 ppm and 375 – 138 ppm), which are inversely correlated with Mg# (Table 2). The

240 basalts LOI values range from 5.8 to 2.4, and most likely reflect the moderately altered nature of
241 these rocks.

242 The chondrite (Anders and Ebihara 1982) normalized REE patterns (Fig. 4a) of the Balagne
243 basalts are characterized by HREE depletion relative to MREE (Gd_N/Yb_N = 1.3-1.2) and moderate
244 LREE enrichment (Ce_N/Sm_N = 1.2-1.0). Bracco-Levanto basalts have HREE patterns nearly parallel
245 to those of Balagne basalts, but show slight LREE depletion relative to MREE (Ce_N/Sm_N = 0.8-0.7).
246 The negative Eu anomaly of both Balagne and Bracco-Levanto basalts is slight to absent and
247 increases with total REE contents (Table 2). The incompatible trace element patterns normalized to
248 chondrite of Balagne basalts display slight enrichment of Zr and Hf relative to REE, Y and Ti, and
249 Nb and Ta depletion with respect to LREE (Fig. 5). Sr overall varies from enriched to depleted
250 relative to adjacent REE, thereby suggesting that Sr concentrations were affected by low
251 temperature alteration. Bracco-Levanto basalts mainly differ in showing a slightly more marked
252 depletion of Nb and Ta relative to LREE. For both Balagne and Bracco-Levanto basalts, the highest
253 concentrations of incompatible trace elements pertain to sample showing the lowest Mg# (i.e.
254 sample N10 and ROS6).

255 We calculated initial ε_{Nd} values of Balagne basalts at 164 Ma, which is the average age proposed
256 for the lower crust of Balagne ophiolite (see section 2). The ε_{Nd} values fall within a restricted range
257 (from +8.8 to +8.6, Table 3, Fig. 6). Bracco-Levanto basalts have homogeneous Nd isotopic
258 compositions with initial ε_{Nd} values calculated at 161 Ma (from +8.8 to +8.6) falling within the
259 same range of Balagne basalts. The ε_{Nd} values yielded by Bracco-Levanto basalts are similar to
260 those obtained by Rampone et al. (1998) and Barry et al. (2017) for basalts from the top of the same
261 basalt-sedimentary succession (+9.1 to +8.6).

262 **Sedimentary rocks**

263 The quartzo-feldspathic sediments from the Balagne ophiolite are arkoses. SiO_2 and Al_2O_3
264 contents range from 71 to 55 wt% and from 14 to 5.0 wt%. The contents of Fe_2O_3, MgO and MnO

are generally low (2.9-1.0 wt%, 1.0-0.7 wt% and ~0.2 wt%). The samples have nearly parallel REE patterns resembling that of NASC (North American Shale 357 Composite, Gromet et al. 1984) and are characterized by a marked LREE enrichment and a slight HREE depletion relative to MREE, and a significant negative Eu anomaly (Fig. 4b). The selected sample of quartzo-feldspathic sediment has enriched Nd isotopic compositions with ε_{Nd} at 164 Ma of -5.5 (Table 3).

The radiolarian cherts have relatively high contents of SiO_2 (~75 wt%), Al_2O_3 (~4.6 wt%), Fe_2O_3 (~9.8 wt%), MgO (~4.7 wt%), CaO (~1.0 wt%) and low of TiO_2 (~0.2 wt%). The concentrations of MnO, V, Cr, Ni, Co and Sc (~0.3 wt%, ~98 ppm, ~345 ppm, ~303 ppm, ~56 ppm and ~8.0 ppm) are relatively high, which could reflect a significant input from hydrothermal deep-sea sediments constituents. In the chondrite-normalized REE diagram the samples show a steady decrease from LREE to HREE, slight Ce depletion relative to La and Pr and moderate negative Eu anomaly (Fig. 4b). The ε_{Nd} of the selected radiolarian chert at the time of the Bracco-Levanto lower crust formation (161 Ma) is -5.2 (Table 3). This value nearly falls within the range of initial ε_{Nd} (-5.3 to -9.1, Stille et al. 1989) found for the cherts from the Platta ophiolitic unit (eastern central Alps).

Clinopyroxene major and trace element chemistry

The Mg# (Table 4) of clinopyroxene from the Balagne and Bracco-Levanto basalts mainly ranges from 78 to 63 and from 82 to 66 (Fig. 7). The concentrations of TiO_2 (2.3–1.2 wt% and 1.3–0.7 wt%) are directly correlated with Al_2O_3 (4.3-2.0 wt% and 3.9-1.6 wt%) and Na_2O (0.7-0.4 wt% and 0.6-0.3). Clinopyroxene from Balagne basalts has overall higher TiO_2 and Na_2O than that from Bracco-Levanto basalts. MnO contents of clinopyroxene from Balagne and Bracco-Levanto basalts are overlapping and overall range from 0.4 to 0.1 wt%, in particular, clinopyroxene with the lowest Mg# has the highest MnO contents (Table 4).

Clinopyroxene from the Balagne basalts has a chondrite-normalized (Anders and Ebihara 1982) REE pattern (Fig. 8) characterized by LREE depletion relative to MREE (Ce_N/Sm_N = 0.4-0.3 for Sm_N = 63-27), negative Eu anomaly (Eu/Eu* 0.8-0.7), and slight depletion of HREE relative to

MREE (Gd_N/Yb_N = 1.5 to 1.4 for Yb_N = 44-21). Normalization to chondrite abundances shows that clinopyroxene has Nb, Ta, Sr, Zr, Hf and Ti depletion relative to adjacent REE (Fig. 9). With respect to clinopyroxene from Balagne, that from Bracco-Levanto is slightly depleted in LREE, MREE, Nb-Ta, Sr, Zr-Hf. Within both ophiolitic successions, clinopyroxene with the lowest Mg# is also characterized by the highest incompatible trace element contents and the most pronounced negative Eu and Sr anomalies.

Discussion

Asthenospheric source and basalt evolution

The Balagne (central-northern Corsica) and Bracco-Levanto (Northern Apennine, eastern Liguria) ophiolites represent a continent-near and an oceanward paleogeographic domain of the Jurassic Liguria-Piedmont ophiolitic basin. They preserve a primary Jurassic association of pillow lavas and massive basalt layers with Middle-Upper Jurassic sediments, mainly constituted by polymict breccias and radiolarian cherts (e.g., Marroni and Pandolfi 2007). In the Balagne ophiolite, in addition, the basalts include levels made up of quartzo-feldspathic clastic sediments derived from Permian continental material (see also Renna et al. 2017).

The Bracco-Levanto basalts locally contain quartz in association with chlorite (Table 1; Fig. 2b). The development of chlorite-quartz assemblage was documented in hydrothermally altered oceanic basalts (e.g., Alt et al. 1986, 1996; Gillis and Thompson 1993) and experimentally reproduced by basalt-seawater interaction (Mottl 1983). The quartz-chlorite associations from the Bracco-Levanto basalts are most likely pseudomorphic after primary clinopyroxene + plagioclase assemblage and produced by interaction with seawater-derived fluids under greenschist facies conditions. Note that clinopyroxene analyses from both Bracco-Levanto and Balagne basalts are consistent. Whole-rock and clinopyroxene trace element compositions, for instance, consistently reveal that the Balagne basalts are slightly enriched in LREE relative to the Ligurian counterparts (Figs. 4 and 8). This

314 indicates that the immobile trace elements and isotope whole rock signatures of basalts were not
315 modified by low temperature hydrothermal alteration processes.

316 The Balagne basalts are slightly enriched in LREE, Nb, Ta, Zr and Hf with respect to typical
317 normal-MORB compositions (Figs. 4 and 5; see also Venturelli et al. 1979), and show affinity to
318 transitional-MORB. The REE patterns of the Bracco-Levanto basalts mostly parallel those typical
319 of normal-MORB (Fig. 4). The basalts from the two ophiolitic successions have homogeneous Nd
320 isotopic compositions with initial ε_{Nd} falling within typical depleted mantle (DM) values and
321 averaging ~+8.7 for both successions. A typical DM-like isotopic signature is also confirmed by the
322 initial ε_{Hf} of +13.6 found for a basalt sample from the top of the Bracco-Levanto succession (Barry
323 et al. 2017). Furthermore, Balagne and Bracco-Levanto basalts overall have relatively high
324 $(Sm/Yb)_{DM}$ values (1.5–1.8, Table 2), which suggest that the depleted mantle source was
325 characterized by a garnet-bearing component (see also Montanini et al. 2008; Saccani et al. 2015).

326 The homogeneous depleted Nd isotopic signature shown by basalts from both Bracco-Levanto
327 and Balagne ophiolitic successions argues against an origin by primitive melts derived from an
328 isotopically enriched lithospheric mantle source. We may also exclude that the parental melts of the
329 basalts experienced assimilation of sediments, as the associated quartzo-feldspathic clastic
330 sediments and radiolarian cherts are characterized by highly radiogenic Nd isotope fingerprints (ε_{Nd}
331 at the time of the basalt formation of -5.5 and -5.2, Table 3). In particular, for the Bracco-Levanto
332 sequence, by assuming +8.7 as the initial ε_{Nd} of the parental mantle-derived melt and a 5 wt%
333 fraction of contaminant material with ε_{Nd} of -5.2, which is equivalent to the modal abundance of
334 quartz in the basalts (Table 1), a ε_{Nd} of +8.0 for the contaminated basalt melt was estimated. This
335 estimate contrasts with the fact that Bracco-Levanto basalts containing minor amounts of quartz
336 have initial ε_{Nd} values of +8.8 to +8.7, which are equivalent to those yielded by the quartz-free
337 basalts (Table 3). Nd isotope data thus confirm that the local occurrence of minor quartz in the
338 Bracco-Levanto basalts was not produced by assimilation of crustal material.

339 Basalts from Bracco-Levanto and Balagne ophiolitic successions have relatively low Mg# (63-37
340 and 65-45), which are lower than those experimentally determined for primary normal-MORB-type
341 melts (Mg# ~76-73, Kinzler and Grove 1992) and overlap the mean composition of mid-ocean
342 ridge basalts (Mg# = 59 ± 7, White and Klein 2014). This indicates that the studied basalts were not
343 in equilibrium with presumed mantle olivine compositions (Mg# = 90; Roeder and Emslie 1970).
344 Within both successions, basalts overall show a decrease of Al_2O_3 and a slight deepening of
345 negative Eu anomaly with decreasing Mg#, thereby suggesting a process controlled by fractional
346 crystallization of clinopyroxene and plagioclase. The decrease of Mg# is also correlated with an
347 increase of TiO_2, MnO and V (Fig. 3, Table 2). In particular, the Balagne and Bracco-Levanto
348 basalts showing the lowest Mg# have TiO_2, FeO^t and FeO^t/MgO values similar to those typical of
349 ferro-basalts (le Roex et al. 1982; Harper 2003). Chemical compositions of clinopyroxene from
350 these ferro-basalts differ in having the lowest Mg# values, the highest incompatible elements
351 concentrations and the most pronounced negative Eu and Sr anomalies (Tables 4 and 5; Figs. 7 to
352 9), thereby confirming the evolved geochemical signature of these rocks.
353 On the basis of clinopyroxene/basalt partition coefficient determined under low-pressure
354 conditions (Shi and Libourel 1991; $K_d Cpx/basalt^{Fe/Mg} = 0.26$), we calculated the Mg# of the melt in
355 equilibrium with the clinopyroxene from the Balagne and Bracco-Levanto ferro-basalts
356 (clinopyroxene Mg# = 65 and 70). Computed Mg# of clinopyroxene equilibrium melts are 32 and
357 38, respectively. Assuming that the fractionation was controlled by separation of clinopyroxene +
358 plagioclase, and starting from a melt with the FeO and MgO composition of the least evolved basalt
359 (Table 2), calculated Mg# yield, for both successions, a degree of fractional crystallization of ~60%.
360 This estimate is confirmed by whole-rock trace elements (La, Ce, Nd, Zr, Sm, Ti, Dy, Y, Yb)
361 modeling. We assumed for the Balagne and Bracco-Levanto basalts a fractional crystallization
362 process with a fractionating assemblage of 0.6 plagioclase + 0.4 clinopyroxene and of 0.5
363 plagioclase + 0.5 clinopyroxene, respectively, in agreement with the estimated modal compositions
364 (Table 1). We also assumed the set of clinopyroxene/melt and plagioclase/melt partition coefficients

365 determined experimentally for a basaltic system (Tiepolo et al. 2002). The compositional range
366 from the most primitive (Mg# = 63) to the most evolved basalt (Mg# = 37) from Balagne was
367 reproduced with F (fraction of remaining liquid) = 0.4 (Fig. 10a). By assuming the whole-rock
368 composition of the least evolved Bracco-Levanto basalt (Mg# = 65), incompatible element
369 compositions of the most evolved ferro-basalt (Mg# = 45) was reproduced assuming F = 0.3 (Fig.
370 10b). For both ophiolitic successions, thus, the development of ferro-basalt compositions involved a
371 process of extensive fractional crystallization.

372 **Chemical variations between basalts as revealed by bulk vs. clinopyroxene chemistry**

373 Clinopyroxene is, together with plagioclase, the main constituent of the basalts and is the main
374 repository for REE and other incompatible trace elements in these rocks. Clinopyroxene from
375 basalts is typically chemically zoned, showing significant core-to-rim variations characterized by an
376 increase of Ti and incompatible trace elements such as Zr, Hf, Nb, Ta, REE, Y, Th and U (Vannucci
377 et al. 1993; Renna et al. 2011). These chemical variations reflect conditions of rapid crystallization,
378 and are thought to be independent of the liquid composition (Claeson et al. 2007) and related to the
379 interplay between crystal-growth phenomena and kinetic effects (Lofgren et al. 2006; Schwandt and
380 McKay 2006). The chemistry of clinopyroxene cores is interpreted to approach the equilibrium
381 conditions and to represent primary compositions of melt giving rise to basalt.

382 In the present study, the compositions of clinopyroxene cores allowed recognition of slight but
383 significant chemical differences between basalts from the Balagne and Bracco-Levanto ophiolites.
384 Clinopyroxenes from the Balagne basalts are enriched in TiO_2 and Na_2O relative to that from the
385 Bracco-Levanto basalts (Fig. 7). Whole rock data (Table 2, Fig. 3) do not exhibit well-defined TiO_2
386 differences between the two successions, which could reflect the influence of Ti-rich clinopyroxene
387 rims and/or Fe-Ti oxides on whole rock compositions. In addition, the bulk Na_2O contents are
388 relatively high for all basalts, which may be likely attributed to the moderate degree of alteration of
389 the samples as reflected in their fairly high L.O.I. values.

390 The most significant differences between Balagne and Bracco-Levanto basalts are the ratios
391 between highly to moderately incompatible trace elements, which remain nearly constant during a
392 differentiation controlled by fractional crystallization of clinopyroxene and plagioclase (± olivine).
393 In particular, clinopyroxene from the Balagne basalts shows higher Ce_N/Sm_N ratios than the
394 clinopyroxene from Bracco-Levanto (0.4-0.3 vs. 0.2). Similarly, bulk data of Balagne basalts show
395 higher Ce_N/Sm_N than Bracco-Levanto (1.2-1.0 vs. 0.8-0.7). Whole-rock analyses of Balagne basalts
396 display higher Nb_N/Y_N and Ta_N/Y_N than Bracco-Levanto counterparts (Nb_N/Y_N = 1.4-0.8 vs. 0.7-0.4
397 and Ta_N/Y_N = 1.7-0.9 vs. 0.5-0.4). Clinopyroxene from the Balagne and Bracco-Levanto basalts
398 does not reveal appreciable differences of Nb_N/Y_N and Ta_N/Y_N ratios, which most likely reflects the
399 low compatibility of these elements for clinopyroxene due to crystal-chemical effects (e.g., Blundy
400 and Wood 1994, Hart and Dunn 1993).
401 Clinopyroxene from the Balagne basalts has higher Zr_N/Y_N and Hf_N/Y_N with respect to that from
402 Bracco-Levanto (Zr_N/Y_N = 0.9-0.6 vs. 0.4-0.3 and Hf_N/Y_N = 1.3-0.9 vs. 0.9-0.5). No substantial Zr-
403 Hf differences are conversely revealed by whole-rock analyses (e.g., Zr_N/Y_N = 2.1-1.6 vs. 1.9-1.3).
404 Late crystallizing portions of clinopyroxene from oceanic basalts and lower oceanic crust generally
405 display variable enrichment of more to less incompatible elements (e.g., Zr/Y) with respect to the
406 inner, early crystallizing mineral portions (e.g., Vannucci et al. 1993; Coogan and O'Hara 2015;
407 Lissenberg et al. 2013; Sanfilippo et al. 2015a). We presume that the significant chemical zoning of
408 clinopyroxene could variably affect the whole rock Zr-Hf budget of the analyzed basalts, thereby
409 decoupling the Zr-Hf signature of clinopyroxene cores and bulk data.
410 In summary, significant chemical differences between Balagne and Bracco-Levanto basalts are
411 shown by both clinopyroxene and bulk data (i.e., LREE and Nb-Ta). Clinopyroxene also enabled to
412 identify chemical differences that are not well-defined by whole rock analyses (i.e., TiO_2, Na_2O and
413 Zr-Hf). Chemical differences are observed for whole-rock and clinopyroxene data with similar Mg#
414 ranges, which imply that these differences are not the result of magmatic evolution. The

415 geochemical signature of Balagne melts was slightly enriched in most incompatible elements
416 (including Na_2O and TiO_2) with respect to that of the Bracco-Levanto parental melts.

417 **Homogeneous vs. heterogeneous mantle sources**

418 The Balagne and Bracco-Levanto basalts show different incompatible element signatures and
419 homogeneous Nd isotopic compositions (Figs. 4 to 6). Numerous geochemical studies generally
420 document highly heterogeneous isotopic and elemental compositions of oceanic basalts, thereby
421 indicating that mantle sources are chemically heterogeneous and consist of complex assemblages of
422 two or more enriched and depleted peridotite components (e.g., Hofmann 2003; Salters and Dick
423 2002; Stracke et al. 2005). The different trace element signature of the basalts from the Bracco-
424 Levanto and Balagne ophiolites may be thus ascribed to melts formed by different amounts of
425 enriched and depleted lithologies in their asthenospheric mantle sources. However, this hypothesis
426 would also require a different Nd isotopic signature for the two basalt series, as the occurrence of
427 enriched sources in the asthenosphere is expected to produce melts with unradiogenic Nd isotopic
428 compositions (Stracke 2012; Wilson et al. 2013).

429 To explain the observed decoupling between the Balagne and Bracco-Levanto basalts, we may
430 hypothesize a process of mixing of partial melts containing different fractions of the various
431 components present within the source, which are both elementally and isotopically distinct. This
432 mixing process should efficiently homogenize the Nd isotopic compositions of the mantle source,
433 whereas heterogeneities in incompatible element ratios were at least partly preserved. Stracke and
434 Bourdon (2009) presented a melting model for heterogeneous mantle (pyroxenites-bearing
435 peridotite) and carried numerical experiments with the aim to investigate how and to what extent
436 isotope and trace element signatures are conveyed from source to melt. They showed that in mixed
437 partial melts differences in highly incompatible trace element ratios are more efficiently averaged
438 than their Nd isotopic compositions. The results by Stracke and Bourdon (2009) thus showed that
439 mixed partial melts, derived from different enriched and depleted mantle components, and

440 characterized by similar Nd isotopic compositions, should also have similar incompatible trace
441 element compositions. We thereby suggest that the different incompatible element signatures, with
442 similar Nd isotopic compositions, shown by the two basalt sequences could not be ascribed to
443 different proportions of enriched and depleted components in their asthenospheric mantle sources.
444 Chemically homogeneous mantle sources therefore provide the most plausible origin for the
445 Balagne and Bracco-Levanto basalts.

446 **Basalt petrogenesis**

447 Two major hypotheses may be formulated to explain the decoupling between incompatible
448 elements and Nd isotopic signatures. In the first, we may postulate that the Balagne and Bracco-
449 Levanto primitive melts formed by different extents of melting of compositionally homogeneous,
450 asthenospheric sources. Accordingly, assuming a homogeneous mantle peridotite source, a different
451 degree of partial melting is suggested by the lower CaO/Al_2O_3 whole-rock ratios shown by Balagne
452 basalts relative to those from Bracco-Levanto (Fig. 11), which is interpreted to indicate origin by
453 lower extent of melting (Klein and Langmuir 1987). This idea is also sustained by the higher
454 Ce_N/Sm_N, Nb_N/Y_N and Ta_N/Y_N ratios shown by the Balagne basalts over Bracco-Levanto. An origin
455 by lower degree of partial melting may also explain the higher TiO_2, Na_2O, Ce_N/Sm_N, Zr_N/Y_N and
456 Hf_N/Y_N exhibited by the clinopyroxene from the Balagne basalts with respect to that from Bracco-
457 Levanto. Furthermore, this petrogenetic hypothesis is reconcilable with the different
458 paleogeographic domains of Balagne and Bracco-Levanto ophiolitic sequences. The Balagne
459 ophiolite is interpreted to represent a continent-near domain, and should therefore be characterized
460 by a colder thermal regime with respect to the oceanward position of the Bracco-Levanto ophiolite.
461 The latter was most likely typified by a hotter mantle, which intersected the solidus deeper and
462 experienced greater extent of melting (Klein 2003) than the colder mantle of the Balagne domain,
463 thereby accounting for the different incompatible elements signatures reflecting different melting
464 degrees.

The second petrogenetic hypothesis implies that primitive melts originally had similar incompatible elements and Nd isotopic signatures, and that a process of interaction between ascending mantle-derived melts and surrounding rocks was subsequently responsible for enriching in highly incompatible elements the parental melts of the Balagne basalts. This process is consistent with compositionally homogeneous partial melts derived by similar melting degrees of the mantle source. Following the melting model by Stracke and Bourdon (2009), however, the proposed process could also be consistent with partial melts derived by enriched and depleted mantle components, which were isotopically and elementally homogenized by mixing process. The petrogenetic hypothesis of interaction between ascending mantle-derived melts and surrounding rocks is suggested by the overall parallel REE and incompatible elements patterns shown by clinopyroxene cores from the Bracco-Levanto basalts and the clinopyroxene cores from lower crustal rocks (i.e. gabbros and olivine-rich troctolites) of the Internal Ligurian ophiolites (Figs. 8-9). This interaction process is generally referred as reactive melt migration and will be discussed in the next section.

Reactive melt migration and the formation of incompatible elements enriched basalts

In modern spreading ridges and ophiolites the process of reaction between ascending MORB-like melts and surrounding rocks has been indicated within (i) the mantle, leading to the formation of impregnated plagioclase peridotite (e.g. Dick et al., 1984; Bonatti et al., 1992; Dygert et al. 2016) and of replacive dunite (e.g., Dick 1977; Kelemen et al. 1995), (ii) at the mantle-crust transitions zone, leading to formation of olivine-rich troctolites (e.g., Suhr et al. 2008; Drouin et al. 2009, 2010; Renna and Tribuzio 2011; Sanfilippo et al 2013, 2015a), and within the lower oceanic crust (e.g., Bédard et al. 2000; Coogan et al. 2000; Gao et al. 2007; Lissenberg and Dick 2008; Renna et al. 2016; Lissenberg and MacLeod 2016). The process of reactive melt migration produces reactive dissolution of pre-existing mineral, modification of the composition of the migrating melt and crystallization of new phases (see also Collier and Kelemen 2010; Lissenberg et al. 2013).

490 Paquet et al. (2016) have recently proposed that the composition of the erupted basalts from the
491 Southwest Indian Ridge (61°-67°E) is controlled by reaction between their parental melts and the
492 surrounding lithospheric mantle rocks (plagioclase-bearing peridotites). This interpretation was
493 explained by the similar trace element signatures found for the erupted basalts and the melts at
494 equilibrium with clinopyroxene from the associated plagioclase-bearing peridotites. The process of
495 melt impregnation of mantle peridotite under plagioclase facies conditions is documented in the
496 mantle section of the Jurassic Alpine ophiolites (e.g., Piccardo et al. 2007; Rampone et al. 2008;
497 Müntener et al. 2010; Sanfilippo and Tribuzio 2011), and it is typically attributed to infiltration of
498 orthopyroxene-saturated melts that caused partial dissolution of mantle clinopyroxene and
499 replacement by plagioclase and orthopyroxene. Note, however, that the chondrite-normalized REE
500 and incompatible trace element patterns of clinopyroxene from the plagioclase-bearing peridotites
501 of the Internal Ligurian ophiolites show marked depletion of LREE, Sr, Zr and Hf with respect to
502 clinopyroxene from the basalts (Figs. 8 and 9). In addition, plagioclase-bearing peridotites have
503 heterogeneous Nd isotopic compositions with ε_{Nd} calculated at the age of the basalt formation that
504 range from +15 to +12 (Rampone et al. 1996, 1998) and thus significantly differ from the
505 homogeneous initial ε_{Nd} value of ~+8.7 found for the basalts. We therefore exclude that the
506 chemical compositions of the basalts were controlled by interaction with mantle rocks.
507 Within the lower oceanic crust, reactive processes typically occur between migrating melts and
508 gabbroic crystal mush (Coogan et al. 2000; Gao et al. 2007; Lissenberg and Dick 2008; Lissenberg
509 et al. 2013). These processes are responsible for the redistribution of incompatible elements from
510 the pre-existing cumulate phases into the interstitial melt and late crystallizing minerals (see also
511 Lissenberg and MacLeod 2016). Olivine-rich troctolites are the most primitive rocks of the lower
512 oceanic crust and their petrogenesis is generally attributed to reaction between an olivine-rich
513 matrix and a migrating MORB-like melt crystallizing mainly plagioclase and clinopyroxene. The
514 origin of the olivine-rich matrix is explained as the production of either magmatic crystallization of
515 primitive melts injected into the growing lower crust or melt-mantle reaction at the mantle-crust

516 transition (cf. Sanfilippo et al. 2015a; Renna et al. 2016). Melt-rock reaction processes have been
517 suggested to explain the major and trace element compositions of olivine from troctolites and
518 olivine-gabbros in different gabbroic sections of the Liguria and Corsica ophiolites (Sanfilippo et al.
519 2014; 2015b). There is general agreement that both gabbros and olivine-rich troctolites from the
520 Liguria and Corsica ophiolites are rocks preserving melt-rock reaction signatures, acquired within
521 the lower crust or at the mantle-crust transition. Gabbro and olivine-rich troctolites of Internal
522 Ligurian ophiolite have $\varepsilon_{Nd\ (161\ Ma)}$ of +8.6 and +8.4 ± 0.3 (Rampone et al. 1998), which are similar
523 to the initial ε_{Nd} value of ~+8.7 found for the Bracco-Levanto basalts. The similar Nd isotopic
524 compositions in tandem with the similar clinopyroxene incompatible elements signatures (Figs. 8
525 and 9) shown by basalts, gabbros and olivine-rich troctolites from Internal Ligurian ophiolites
526 therefore suggest that the interaction with the lower crustal crystal mush could affect the chemical
527 composition of basalt parental melts.
528 The cores of clinopyroxenes from gabbros and olivine-rich troctolites of Jurassic Alpine
529 ophiolites display a range of Ce_N/Sm_N ratios that encompass the values of Ce_N/Sm_N shown by the
530 clinopyroxene cores from the Balagne and Bracco-Levanto basalts (Fig. 12). With respect to
531 clinopyroxene cores from gabbros and olivine-rich troctolites of Jurassic Alpine ophiolites and to
532 those from Bracco-Levanto basalts, however, the Balagne clinopyroxene cores differ in having
533 higher Zr_N/Y_N ratios. The latter values are, in particular, comparable to those shown by the rims of
534 clinopyroxenes from gabbros and olivine-rich troctolites of Jurassic Alpine ophiolites. The
535 enrichment of incompatible elements (e.g., Ti, Zr, and REE) from core to rim of clinopyroxene has
536 been observed in oceanic gabbros and olivine-rich troctolites and ascribed to crystallization from
537 reactive melts dissolving a pre-existing crystal assemblage (Lissenberg and Dick 2008; Coogan et
538 al. 2000; Gao et al. 2007; Coogan 2007; Lissenberg et al. 2013; Sanfilippo et al. 2015a).
539 Enrichments of incompatible elements, associated with increasing degree of fractionation between
540 incompatible elements (e.g., Zr to Y), are explained by an AFC (assimilation and concomitant
541 fractional crystallisation) process involving assimilation by the reactively migrating MORB-like

542 melt of (i) various proportion of early crystallized olivine, plagioclase and clinopyroxene for
543 oceanic gabbros, and (ii) mantle peridotites for olivine-rich troctolites. Within the context of gabbro
544 evolution, in particular, it is proposed that migrating melts become increasingly more evolved and
545 trace elements-enriched by the reactive process, thereby promoting the crystallization of trace
546 elements-enriched clinopyroxene marginal portions and leaving depleted olivine, plagioclase and
547 clinopyroxene cores.

548 Lissenberg et al. (2013) proposed a model for melt evolution in the lower oceanic crust with the
549 following sequence of events: (i) mantle-derived melts form a crystal mush of olivine, plagioclase
550 and clinopyroxene; (ii) some residual MORB-like melts may be rapidly extracted, escape melt-rock
551 reaction and may locally erupt; (iii) the remainder MORB-like melts reactively migrate within the
552 crystal mush; incompatible elements are redistributed from the cumulate minerals into the migrating
553 melts, which become increasingly enriched in most incompatible elements and result in
554 crystallization of enriched clinopyroxene rims (and other late crystallizing accessory minerals); (iv)
555 the residual, evolved and incompatible elements-enriched melt is delivered to shallow level melt
556 lens where it may mix with the unreacted MORB-like melt prior to eruption. The proposed scenario
557 result in the eruption of basalts ranging from depleted to variably enriched in most incompatible
558 elements. We speculate that a similar petrogenetic sequence of events may be envisaged to explain
559 the decoupling between incompatible elements and Nd isotopic signature of Bracco-Levanto and
560 Balagne basalts. The reactive process less efficiently modifies the ratios of Sm/Nd relative to those
561 between highly to moderately incompatible elements (e.g. Zr/Y), because Sm and Nd have a similar
562 geochemical behavior. The chemical compositions of Bracco-Levanto and Balagne basalts could be
563 thus controlled by the interaction with the lower crustal crystal mush, which had similar Nd isotopic
564 signature and therefore did not modify the Nd isotopic composition of primitive basalt melts. The
565 slight enrichment in highly incompatible elements shown by the Balagne relative to Bracco-Levanto
566 basalts may be explained by a higher contribute, in Balagne parental basalt melts, of more evolved
567 and slightly more trace elements-enriched reactively migrating melts.

During the process of reactive melt migration, the reactively migrating melts become progressively more evolved and enriched in incompatible trace elements due to the local assimilation of crystal phases and synchronous crystallization at decreasing melt mass (Lissenberg et al. 2013). It implies that a melt reactively migrating within a crystal mush with a relatively high melt/crystal ratio has a lower enrichment in incompatible elements than a melt reactively migrating within a crystal mush characterized by a lower melt/crystal ratio. We may speculate that the two different trace element signatures of the Balagne and Bracco-Levanto basalts reflected different melt/crystal ratios of the crystal mush, namely the primitive melts giving rise to the Bracco-Levanto basalts interacted with a crystal mush characterized by a higher melt/crystal ratio with respect to the crystal mush that interacted with the Balagne primitive melts. These different melt/crystal ratios of the crystal mush could reflect the different thermal conditions between the continent-near Balagne domain and the oceanward position of Bracco-Levanto ophiolite.

8 Summary and concluding remarks

The Balagne (central-northern Corsica, France) and Bracco-Levanto (northern Apennine, Italy) ophiolites are respectively marginal and oceanward fragments of a Jurassic slow or ultraslow spreading basin, commonly referred as Liguria-Piedmont basin. These ophiolitic bodies expose thick basalt sequences typically associated with Middle-Upper Jurassic sediments, mainly polymict breccias and radiolarian cherts (e.g., Marroni and Pandolfi 2007). In addition, continent-derived clastic sediments are included within the Balagne basalt sequence (see also Renna et al. 2017).

The basalts from the two ophiolites have slightly different incompatible elements signatures, as consistently shown by both whole-rock and clinopyroxene compositions. Normal-MORB affinity characterizes the Bracco-Levanto basalts, whereas transitional-MORB typifies the Balagne basalts. The two basalt successions, however, have similar initial Nd isotopic compositions, plotting within typical depleted mantle values. The primitive melts giving rise to the two basalt successions formed by an asthenospheric mantle source likely containing a garnet-bearing enriched component. The

magmatic evolution of both basalt successions included a stage of protracted crystallization ruled by separation of clinopyroxene and plagioclase, which finally led to melts with ferro-basaltic compositions.

The decoupling between incompatible elements and Nd isotopic signatures could reflect different degrees of partial melting from similar mantle sources. Alternatively, the decoupled incompatible trace elements and Nd isotope compositions were acquired by a process of reactive melt migration within a lower crustal crystal mush. Both hypotheses are reconcilable with the interpretation that the Balagne and Bracco-Levanto basaltic sequences formed in continent-near and oceanward domains of a nascent oceanic basin.

Acknowledgments

We are grateful to V. Salters and an anonymous reviewer for the constructive comments that considerably improved the quality of this study. This work was financially supported by Programma di Ricerca di Interesse Nazionale of the Italian Ministero dell'Università e della Ricerca, and Fondi Ricerca Giovani of Università degli Studi di Pavia.

609 ## References

610 Abbate E, Bortolotti V, Principi G (1980) Apennine ophiolites: a peculiar oceanic crust. Ofioliti 1:
611 59-96.

612 Alt JC, Honnorez J, Laverne C, Emmermann R (1986) Hydrothermal alteration of a 1 km section
613 through the upper oceanic crust, Deep Sea Drilling Project Hole 504B: Mineralogy, chemistry
614 and evolution of seawater-basalt interactions. J Geophys Res-Sol Ea, 91: 10309-10335

615 Alt JC, Laverne C, Vanko DA, Tartarotti P, Teagle DA, Bach W, Zuleger E, Erzinger J, Honnorez
616 J, Pezard PA, Becker K, Salisbury MH, Becker K (1996). 34. Hydrothermal alteration of a
617 section of upper oceanic crust in the Eastern Equatorial Pacific: a synthesis of results from site
618 504 (DSDP LEGS 69, 70, and 83, and ODP LEGS 111, 137,140, and 148). Proceedings of the
619 Ocean Drilling Program, Scientific Results, Vol. 148

620 Anders E, Ebihara M. (1982). Solar-system abundances of the elements. Geochim Cosmochim
621 Ac 46: 2363-2380

622 Barry TL, Davies JH, Wolstencroft M, Millar IL, Zhao Z, Jian P, Safanova I, Price M (2017).
623 Whole-mantle convection with tectonic plates preserves long-term global patterns of upper
624 mantle geochemistry. Sci Rep 7: 1870

625 Baud J.P. (1975) Étude géologique du massif de roches vertes de Haute-Balagne (Corse). PhD
626 thesis

627 Bédard JH (2000) Betts Cove ophiolite and its cover rocks, Newfoundland. Natural Resources
628 Canada, No. 550.

629 Bill M, O'Dogherty L, Guex J, Baumgartner PO, Masson H (2001) Radiolarite ages in Alpine-
630 Mediterranean ophiolites: constraints on the oceanic spreading and the Tethys-Atlantic
631 connection. Geol Soc Am Bull 113: 129–143

632 Blichert-Toft J, Rosing MT, Lesher CE, Chauvel C (1995) Geochemical constraints on the origin of
633 the late Archean Skjoldungen Alkaline Igneous Province, SE Greenland. J Petrol 36: 515-561

634 Blundy J, Wood B (1994) Prediction of crystal–melt partition coefficients from elastic moduli.
635 Nature 372: 452-454
636 Bonatti E, Peyve A, Kepezhinskas P, Kurentsova N, Seyler M, Skolotnev S, Udintsev G (1992)
637 Upper mantle heterogeneity below the Mid-Atlantic Ridge, 0–15 N. J Geophys Res-Sol Ea 97:
638 4461-4476
639 Borghini G, Rampone E (2007) Postcumulus processes in oceanic-type olivine-rich cumulates: the
640 role of trapped melt crystallization versus melt/rock interaction. Contrib Mineral Petr 154: 619-
641 633
642 Chiari M, Marcucci M, Principi G (2000) The age of the radiolarian cherts associated with the
643 ophiolites in the Apennines (Italy). Ofioliti 25: 141–146
644 Claeson DT, Meurer WP, Hogmalm KJ, Larson SÅ (2007) Using LA-ICPMS mapping and sector
645 zonation to understand growth and trace-element partitioning in sector-zoned clinopyroxene
646 oikocrysts from the Norra Ulvö Gabbro, Sweden. J Petrol 48: 711-728
647 Collier ML, Kelemen PB (2010) The case for reactive crystallization at mid-ocean ridges. J Petrol
648 51: 1913-1940
649 Coogan LA, Saunders AD, Kempton PD, Norry MJ (2000) Evidence from oceanic gabbros for
650 porous melt migration within a crystal mush beneath the Mid-Atlantic Ridge. Geochem Geophy
651 Geosy 1: Paper number 2000GC000072
652 Coogan LA, O'Hara MJ (2015) MORB differentiation: In situ crystallization in replenished-tapped
653 magma chambers. Geochim Cosmochim Ac 158: 147-161
654 Cortesogno L, Galbiati B, Principi G (1987) Note alla "carta geologica delle ofioliti del Bracco" e
655 ricostruzione della paleogeografia giurassico-cretacea. Ofioliti 12: 261-342
656 Danelian T, De Wever P, Durand-Delga M (2008) Revised radiolarian ages for the sedimentary
657 cover of the Balagne ophiolite (Corsica, France). Implications for the palaeoenvironmental
658 evolution of the Balano-Ligurian margin. B Soc Geol Fr 179: 289-296

659 Desmurs L, Müntener O, Manatschal G (2002) Onset of magmatic accretion within a magma-poor
660 rifted margin: a case study from the Platta ocean-continent transition, eastern
661 Switzerland. Contrib Mineral Petr, 144(3): 365-382
662 Dick HJ (1977) Partial melting in the Josephine Peridotite; I, The effect on mineral composition and
663 its consequence for geobarometry and geothermometry. Am J Sci 277: 801-832
664 Dick HJ, Fisher RL, Bryan WB (1984) Mineralogic variability of the uppermost mantle along mid-
665 ocean ridges. Earth Planet Sc Lett 69: 88-106.
666 Drouin M, Godard M, Ildefonse B, Bruguier O, Garrido CJ (2009) Geochemical and petrographic
667 evidence for magmatic impregnation in the oceanic lithosphere at Atlantis Massif, Mid-Atlantic
668 Ridge (IODP Hole U1309D, 30 N). Chem Geol 264: 71-88
669 Drouin M, Ildefonse B, Godard M (2010) A microstructural imprint of melt impregnation in slow
670 spreading lithosphere: Olivine-rich troctolites from the Atlantis Massif, Mid-Atlantic Ridge, 30
671 N, IODP Hole U1309D. Geochem Geophy Geosy 11: Q06003, doi:10.1029/2009GC002995
672 Durand-Delga M. (1984) Principaux traits de la Corse Alpine et corrélations avec les Alpes Ligures.
673 Memorie della Società Geologica Italiana 28: 285–329
674 Durand-Delga M, Peybernès B, Rossi P (1997) Arguments en faveur de la position, au Jurassique,
675 des ophiolites de Balagne (Haute-Corse, France) au voisinage de la marge continentale
676 européenne. Cr Acad Sci II A, 325: 973-981
677 Durand-Delga M, Lahondère D, Puccinelli A, Rossi P, Vellutini P (2001) Pre-Meeting transect
678 Corsica-Elba Isalndsouthern Tuscany Guidebook-Corsica. Ofioliti 26: 303-320
679 Dygert N, Liang Y, Kelemen PB (2016) Formation of plagioclase lherzolite and associated dunite–
680 harzburgite–lherzolite sequences by multiple episodes of melt percolation and melt–rock
681 reaction: an example from the Trinity Ophiolite, California, USA. J Petrol 57: 815-838
682 Gale A, Dalton CA, Langmuir CH, Su Y, Schilling JG (2013) The mean composition of ocean ridge
683 basalts. Geochem Geophy Geosy 14: 489-518

684 Gao Y, Hoefs J, Hellebrand E, von der Handt A, Snow JE (2007) Trace element zoning in
685 pyroxenes from ODP Hole 735B gabbros: diffusive exchange or synkinematic crystal
686 fractionation?. Contrib Mineral Petr 153: 429-442
687 Gillis KM, Thompson G, Kelley DS (1993) A view of the lower crustal component of hydrothermal
688 systems at the Mid-Atlantic Ridge. J Geophys Res-Sol Ea, 98: 19597-19619
689 Gromet LP, Haskin LA, Korotev RL, Dymek RF (1984). The "North American shale composite":
690 its compilation, major and trace element characteristics. Geochim Cosmochim Ac 48: 2469-2482
691 Grove TL, Kinzler RJ, Bryan WB (1993) Fractionation of mid-ocean ridge basalt (MORB). Mantle
692 flow and melt generation at mid-ocean ridges, 281-310
693 Gruppo di Lavoro sulle Ofioliti Mediterranee (1977) I complessi ofiolitici e le unità cristalline della
694 Corsica alpina. Ofioliti 2: 265–324
695 Harper GD (2003) Fe-Ti basalts and propagating-rift tectonics in the Josephine Ophiolite. Geol Soc
696 Am Bull 115: 771-787
697 Hart SR, Dunn T (1993) Experimental cpx/melt partitioning of 24 trace elements. Contrib Mineral
698 Petr 113: 1-8
699 Hemond C, Hofmann AW, Vlastelic I, Nauret F (2006) Origin of MORB enrichment and relative
700 trace element compatibilities along the mid-Atlantic Ridge between 10 and 24 N. Geochem
701 Geophy Geosy 7(12): Q12010, doi:10.1029/2006GC001317
702 Hirschmann MM, Stolper, EM (1996) A possible role for garnet pyroxenite in the origin of the
703 "garnet signature" in MORB. Contrib Mineral Petr 124: 185-208
704 Hofmann AW (2003) Sampling mantle heterogeneity through oceanic basalts: isotopes and trace
705 elements. Treatise on geochemistry 2: 61-101
706 Jeffries, T. E., Jackson, S. E., & Longerich, H. P. (1998). Application of a frequency quintupled Nd:
707 YAG source (λ= 213 nm) for laser ablation inductively coupled plasma mass spectrometric
708 analysis of minerals. J Anal Atom Spectrom 13: 935-940

709 Kelemen PB, Shimizu N, Salters VJ (1995) Extraction of mid-ocean-ridge basalt from the
710 upwelling mantle by focused flow of melt in dunite channels. Nature 375: 747-753
711 Kinzler RJ, Grove TL (1992) Primary magmas of mid-ocean ridge basalts 1. Experiments and
712 methods. J Geophys Res-Sol Ea 97: 6885-6906
713 Klein EM, Langmuir CH (1987) Global correlations of ocean ridge basalt chemistry with axial
714 depth and crustal thickness. J Geophys Res-Sol Ea 92: 8089-8115
715 Klein EM (2003) Geochemistry of the igneous oceanic crust. Treatise on geochemistry 3, 433-463.
716 Kretz R (1983) Symbols for rock-forming minerals. Am mineral 68: 277-279
717 Lagabrielle Y, Cannat M (1990) Alpine Jurassic ophiolites resemble the modern central Atlantic
718 basement. Geology 18: 319-322
719 Le Maitre RW (1989) A classification of igneous rocks and glossary of terms. Blackwell, Oxford
720 Le Roex AP, Dick HJB, Reid AM, Erlank AJ (1982) Ferrobasalts from the Spiess ridge segment of
721 the Southwest Indian ridge. Earth Planet Sc Lett 60: 437-451
722 Le Roux PJ, le Roex A, Schilling J-G, Shimizu N, Perkins WW, Pearce NJG (2002) Mantle
723 heterogeneity beneath the southern Mid-Atlantic Ridge: Trace element evidence for
724 contamination of ambient asthenospheric mantle. Earth Planet Sc Lett 203: 479-498
725 Li XH, Faure M, Rossi P, Lin W, Lahondere D (2015) Age of Alpine Corsica ophiolites revisited:
726 Insights from in situ zircon U–Pb age and O–Hf isotopes. Lithos 220: 179-190
727 Lissenberg CJ, Dick HJ (2008) Melt–rock reaction in the lower oceanic crust and its implications
728 for the genesis of mid-ocean ridge basalt. Earth Planet Sc Lett 271: 311-325
729 Lissenberg CJ, MacLeod CJ, Howard KA, Godard M (2013) Pervasive reactive melt migration
730 through fast-spreading lower oceanic crust (Hess Deep, equatorial Pacific Ocean). Earth Planet
731 Sc Lett 361: 436-447
732 Lissenberg CJ, MacLeod CJ (2016) A reactive porous flow control on mid-ocean ridge magmatic
733 evolution. J Petrol 57: 2195-2220

734 Lofgren GE, Huss GR, Wasserburg GJ (2006) An experimental study of trace-element partitioning
735 between Ti-Al-clinopyroxene and melt: Equilibrium and kinetic effects including sector zoning.
736 Am Mineral 91: 1596-1606
737 Manatschal G, Müntener O. (2009) A type sequence across an ancient magma-poor ocean–
738 continent transition: the example of the western Alpine Tethys ophiolites. Tectonophysics 473:
739 4-19
740 Marroni M, Pandolfi L (2003) Deformation history of the ophiolite sequence from the Balagne
741 Nappe, northern Corsica: insights in the tectonic evolution of Alpine Corsica. Geol J 38: 67-83
742 Marroni M, Pandolfi L (2007) The architecture of an incipient oceanic basin: a tentative
743 reconstruction of the Jurassic Liguria-Piemonte basin along the Northern Apennines–Alpine
744 Corsica transect. Int J Earth Sci 96: 1059-1078
745 Meyzen CM, Toplis MJ, Humler E, Ludden JN, Mével C (2003) A discontinuity in mantle
746 composition beneath the southwest Indian ridge. Nature 421: 731-733
747 Molli G, Malavieille J (2011) Orogenic processes and the Corsica/Apennines geodynamic
748 evolution: insights from Taiwan. Int J Earth Sci 100: 1207-1224
749 Montanini A, Tribuzio R, Vernia L (2008) Petrogenesis of basalts and gabbros from an ancient
750 continent–ocean transition (External Liguride ophiolites, Northern Italy). Lithos 101: 453-479
751 Mottl MJ (1983) Metabasalts, axial hot springs, and the structure of hydrothermal systems at mid-
752 ocean ridges. Geol Soc Am Bull 94: 161-180
753 Müntener O, Manatschal G, Desmurs L, Pettke T (2010) Plagioclase peridotites in ocean–continent
754 transitions: refertilized mantle domains generated by melt stagnation in the shallow mantle
755 lithosphere. J Petrol 51: 255-294
756 O'neill HSC, Jenner FE (2012) The global pattern of trace-element distributions in ocean floor
757 basalts. Nature 491: 698-705

758 Paquet M, Cannat M, Brunelli D, Hamelin C, Humler E (2016) Effect of melt/mantle interactions
759 on MORB chemistry at the easternmost Southwest Indian Ridge (61°–67° E). Geochem Geophy
760 Geosy 17: 4605-4640
761 Peybernès B, Durand-Delga M, Cugny P (2001) Reconstitution, en Corse, au Jurassique moyen–
762 supérieur, de la marge européenne de l'océan Liguro-Piémontais, grâce à des niveaux repères à
763 Praekurnubia crusei (foraminifère). Cr Acad Sci II A 332: 499–506
764 Piccardo GB, Zanetti A, Müntener O (2007) Melt/peridotite interaction in the Southern Lanzo
765 peridotite: field, textural and geochemical evidence. Lithos 94: 181-209
766 Principi G, Bortolotti V, Chiari M, Cortesogno L, Gaggero L, Marcucci M, Saccani E, Treves B
767 (2004) The pre-orogenic volcano-sedimentary covers of the Western Tethys oceanic basin: a
768 review. Ofioliti 29: 177-212
769 Rampone E, Hofmann AW, Piccardo GB, Vannucci R, Bottazzi P, Ottolini L (1996) Trace element
770 and isotope geochemistry of depleted peridotites from an N-MORB type ophiolite (Internal
771 Liguride, N. Italy). Contrib Mineral Petr 123: 61-76
772 Rampone E, Piccardo GB, Vannucci R, Bottazzi P (1997) Chemistry and origin of trapped melts in
773 ophioiitic peridotites. Geochim Cosmochim Ac 61: 4557-4569
774 Rampone E, Hofmann AW, Raczek I (1998) Isotopic contrasts within the Internal Liguride
775 ophiolite (N. Italy): the lack of a genetic mantle–crust link. Earth Planet Sc Lett 163: 175-189
776 Rampone E, Piccardo GB, Hofmann AW (2008) Multi-stage melt–rock interaction in the Mt.
777 Maggiore (Corsica, France) ophiolitic peridotites: microstructural and geochemical evidence.
778 Contrib Mineral Petr 156: 453-475
779 Regelous M, Weinzierl CG, Haase KM (2016) Controls on melting at spreading ridges from
780 correlated abyssal peridotite–mid-ocean ridge basalt compositions. Earth Planet Sc Lett 449: 1-
781 11
782 Renna MR, Tribuzio R (2011) Olivine-rich troctolites from Ligurian ophiolites (Italy): evidence for
783 impregnation of replacive mantle conduits by MORB-type melts. J Petrol 52: 1763–1790

784 Renna MR, Tiepolo M, Tribuzio R (2011) In situ U-Pb geochronology of baddeleyite-zircon pairs
785 using laser-ablation ICPMS: the case-study of quartz gabbro from Varney Nunatak (central
786 Victoria Land, Antarctica). Eur J Mineral 23: 223-240
787 Renna MR, Tribuzio R, Ottolini L (2016) New perspectives on the origin of olivine-rich troctolites
788 and associated harrisites from the Ligurian ophiolites (Italy). J Geol Soc London 173: 916-932
789 Renna MR, Tribuzio R, Sanfilippo A, Tiepolo M (2017) Zircon U–Pb geochronology of lower crust
790 and quartzo-feldspathic clastic sediments from the Balagne ophiolite (Corsica). Swiss J
791 Geosci 110: 479-501
792 Roeder PL, Emslie R (1970) Olivine-liquid equilibrium. Contrib Mineral Petr 29: 275-289
793 Rossi P, Durand-Delga M, Lahondere JC (2001) Carte Géologique de France (1/50000), feuille
794 Santo-Pietro-di-Tenda (1106). In: Orleans BRGM. Notice explicative par (eds Rossi, P., Durand-
795 Delga, M., Lahondere, J. C. & Lahondere, D.), 224. BRGM Orléans, France
796 Rossi P, Cocherie A, Lahondère D, Fanning C.M. (2002) La marge européenne de la Téthys
797 jurassique en Corse: datation de trondhjémites de Balagne et indices de croûte continentale sous
798 le domaine Balano-Ligure. C R Geosci 334: 313-322
799 Saccani E, Principi G, Garfagnoli F, Menna F (2008) Corsica ophiolites: geochemistry and
800 petrogenesis of basaltic and metabasaltic rocks. Ofioliti 33: 187-207
801 Saccani E (2015) A new method of discriminating different types of post-Archean ophiolitic basalts
802 and their tectonic significance using Th-Nb and Ce-Dy-Yb systematics. Geosci Front 6: 481-501
803 Salters VJ, Dick HJ (2002) Mineralogy of the mid-ocean-ridge basalt source from neodymium
804 isotopic composition of abyssal peridotites. Nature 418: 68-72
805 Sanfilippo A, Tribuzio R (2011) Melt transport and deformation history in an ‘‘non-volcanic’’
806 ophiolitic section (Northern Apennine, Italy): implications for crustal accretion at slow spreading
807 settings. *Geochem Geophy Geosy* 12: Q0AG04, http://doi: 101029/2010GC003429
808 Sanfilippo A, Dick HJ, Ohara Y (2013) Melt–rock reaction in the mantle: mantle troctolites from
809 the Parece Vela ancient back-arc spreading center. J Petrol 54: 861-885

Sanfilippo A, Tribuzio R, Tiepolo M (2014) Mantle–crust interactions in the oceanic lithosphere: Constraints from minor and trace elements in olivine. Geochim Cosmochim Ac 141: 423-439

Sanfilippo A, Morishita T, Kumagai H, Nakamura K, Okino K, Hara K, Tamura A, Arai S (2015a) Hybrid troctolites from mid-ocean ridges: inherited mantle in the lower crust. Lithos 232: 124-130

Sanfilippo A, Tribuzio R, Tiepolo M, Berno D (2015b) Reactive flow as dominant evolution process in the lowermost oceanic crust: evidence from olivine of the Pineto ophiolite (Corsica). Contrib Mineral Petrol 170: 1-12

Schwandt CS, McKay GA (2006) Minor-and trace-element sector zoning in synthetic enstatite. Am Mineral 91: 1607-1615

Schwarzenbach EM, Früh-Green GL, Bernasconi SM, Alt JC, Shanks III WC, Gaggero L, Crispini L (2012) Sulfur geochemistry of peridotite-hosted hydrothermal systems: comparing the Ligurian ophiolites with oceanic serpentinites. Geochim Cosmochim Ac 91: 283-305

Shi P, Libourel G. (1991) The effects of FeO on the system CMAS at low pressure and implications for basalt crystallization processes. Contrib Mineral Petr 108: 129-145

Standish JJ, Dick HJB, Michael PJ, Melson WG, O'Hearn T (2008) MORB generation beneath the ultraslow spreading Southwest Indian Ridge (9–25 E): Major element chemistry and the importance of process versus source. Geochem Geophy Geosy 9: Q05004

Stille P, Clauer N, Abrecht J (1989) Nd isotopic composition of Jurassic Tethys seawater and the genesis of Alpine Mn-deposits: Evidence from Sr-Nd isotope data. Geochim Cosmochim Ac 53: 1095-1099

Stracke A, Hofmann AW, Hart SR (2005) FOZO, HIMU, and the rest of the mantle zoo. Geochem Geophy Geosy 6: Q05007

Stracke A, Bourdon B (2009) The importance of melt extraction for tracing mantle heterogeneity. Geochim Cosmochim Ac 73: 218-238

835 Stracke A. (2012) Earth's heterogeneous mantle: A product of convection-driven interaction
836 between crust and mantle. Chem Geol 330: 274-299
837 Suhr G, Hellebrand E, Johnson K, Brunelli D (2008) Stacked gabbro units and intervening mantle:
838 A detailed look at a section of IODP Leg 305, Hole U1309D. Geochem Geophy Geosy 9:
839 Q10007, doi:10.1029/2008GC002012
840 Thirlwall MF (1991a) Long-term reproducibility of multicollector Sr and Nd isotope ratio
841 analysis. Chemical Geology: Isotope Geoscience section 94: 85-104
842 Thirlwall MF (1991b) High-precision multicollector isotopic analysis of low levels of Nd as
843 oxide. Chem Geol 94: 13-22
844 Tiepolo M, Tribuzio R, Vannucci R (2002) The compositions of mantle-derived melts developed
845 during the Alpine continental collision. Contrib Mineral Petr 144: 1-15
846 Treves BE, Harper GD (1994) Exposure of serpentinites on the ocean floor: sequence of faulting
847 and hydrofracturing in the Northern Apennine ophicalcites. Ofioliti 19: 435-466
848 Tribuzio R, Riccardi MP, Ottolini L (1995) Trace element redistribution in high-temperature
849 deformed gabbros from East Ligurian ophiolites (Northern Apennines, Italy): constraints on the
850 origin of syndeformation fluids. J Metamorph Geol 13: 367-377
851 Tribuzio R, Tiepolo M, Vannucci R, Bottazzi P (1999) Trace element distribution within olivine-
852 bearing gabbros from the Northern Apennine ophiolites (Italy): evidence for post-cumulus
853 crystallization in MOR-type gabbroic rocks. Contrib Mineral Petr 134: 123-133
854 Tribuzio R, Renna MR, Dallai L, Zanetti A (2014) The magmatic–hydrothermal transition in the
855 lower oceanic crust: Clues from the Ligurian ophiolites, Italy. Geochim Cosmochim Ac 130:
856 188-211
857 Tribuzio R, Garzetti F, Corfu F, Tiepolo M, Renna MR (2016) U–Pb zircon geochronology of the
858 Ligurian ophiolites (Northern Apennine, Italy): Implications for continental breakup to slow
859 seafloor spreading. Tectonophysics 666: 220-243

860 Vannucci R, Rampone E, Piccardo GB, Ottolini L, Bottazzi P (1993) Ophiolitic magmatism in the
861 Ligurian Tethys: an ion microprobe study of basaltic clinopyroxenes. Contrib Mineral Petr 115:
862 123-137
863 Venturelli G, Thorpe RS, Potts PJ (1981) Rare earth and trace element characteristics of ophiolitic
864 metabasalts from the Alpine-Apennine belt. Earth Planet Sc Lett 53: 109-123
865 Vissers RL, van Hinsbergen DJ, Meijer PT, Piccardo GB (2013) Kinematics of Jurassic ultra-slow
866 spreading in the Piemonte Ligurian ocean. Earth Planet Sc Lett 380: 138-150
867 Waters CL, Sims KW, Perfit MR, Blichert-Toft J, Blusztajn J (2011) Perspective on the genesis of
868 E-MORB from chemical and isotopic heterogeneity at 9–10 N East Pacific Rise. J Petrol 52:
869 565-602
870 White WM, Klein EM (2014) 4.13 - Composition of the Oceanic Crust. Treatise on Geochemistry
871 (Second Edition). 457-496
872 Wilson SC, Murton BJ, Taylor RN (2013) Mantle composition controls the development of an
873 Oceanic Core Complex. Geochem Geophy Geosy 14(4): 979-995
874

875 **Figure captions**

876 **Fig. 1** (a) Geological sketch map of the main ophiolitic bodies of the Northern Apennine, Western
877 Alps and Corsica (slightly modified after Sanfilippo et al. 2014) and geographical location of the
878 Balagne and Bracco-Levanto ophiolites (red squares). (b) and (c) Stratigraphic reconstruction of the
879 Balagne and Bracco-Levanto basalt-sedimentary sequences, and location of selected samples (light
880 blue star). In (b), a simplified reconstruction of the Moltifao slice (not to scale) is also shown and
881 correlated to the main basalt-sedimentary section assuming that the gabbros in the lowermost part of
882 the Moltifao slice represent the substrate of the Balagne ophiolite (see also Renna et al. 2017).

883

884 Fig. 2 Thin section photomicrographs: (a) poikilitic clinopyroxene (Cpx) partially replaced by
885 chlorite (Chl) and enclosing altered plagioclase (Pl), (sample RF2); anhedral quartz (Qtz) rimmed
886 by chlorite and enclosing acicular apatite (Ap), (sample ROS6).

887

888 **Fig. 3** Major element whole-rock variation (calculated water free): TiO_2 versus Mg#.

889

890 **Fig. 4** Whole-rock REE compositions of the basalts (a) and (b) the associated sedimentary rocks
891 normalized to chondrite (Anders and Ebihara 1982). The compositions of normal- and enriched-
892 MORB (N- and E-MORB, Gale et al. 2013), and of NASC (North American Shale Composite,
893 Gromet et al. 1984) are reported for comparative purposes.

894

895 **Fig. 5** Whole-rock incompatible trace element compositions of the basalts, normalized to chondrite
896 (Anders and Ebihara 1982). The compositions of normal- and enriched-MORB (N- and E-MORB,
897 Gale et al. 2013) are reported for comparative purposes.

898

899 **Fig. 6** Plot of initial ε_{Nd} versus $^{147}Sm/^{144}Nd$. Initial ε_{Nd} and $^{147}Sm/^{144}Nd$ values of basalts from the
900 top of the Bracco-Levanto succession after Rampone et al. (1998) are also shown.
901
902 **Fig. 7** Variation of Mg#, Al_2O_3 and Na_2O versus TiO_2 in the clinopyroxene cores.
903
904 **Fig. 8** REE compositions of the clinopyroxene cores, normalized to chondrite (Anders and Ebihara
905 1982). The REE compositions of clinopyroxene cores from plagioclase-rich peridotites (Rampone
906 et al. 1997; Sanfilippo and Tribuzio 2011), olivine-rich troctolites (shaded grey area, Renna and
907 Tribuzio 2011) and gabbros (Sanfilippo and Tribuzio 2011; Tribuzio et al. 2014) from Internal
908 Ligurian ophiolites are also reported for comparative purposes.
909
910 **Fig. 9** Chondrite normalized (Anders and Ebihara 1982) incompatible trace element compositions
911 of the clinopyroxene cores. The incompatible trace element compositions of clinopyroxene cores
912 from plagioclase-rich peridotites (Rampone et al., 1997; Sanfilippo and Tribuzio 2011), olivine-rich
913 troctolites (shaded grey area, Renna and Tribuzio 2011) and gabbros (Sanfilippo and Tribuzio 2011;
914 Tribuzio et al. 2014) from Internal Ligurian ophiolites are also reported for comparative purposes.
915
916 **Fig. 10** Incompatible trace elements (La, Ce, Nd, Zr, Sm, Ti, Dy, Y, Yb) compositions of melts
917 calculated through a process of fractional crystallization, normalized to average N-MORB (Gale et
918 al. 2013). The set of mineral/liquid partition coefficients experimentally determined and reported in
919 Tiepolo et al. (2002) were used. $^{Cpx/liq}D$ values are: La = 0.05, Ce = 0.09, Nd = 0.2, Zr = 0.1, Sm =
920 0.33, Ti = 0.28, Dy = 0.45, Y = 0.43, Yb = 0.39. $^{Pl/liq}D$ values are: La = 0.217, Ce = 0.166, Nd =
921 0.138, Zr = 0.001, Sm = 0.124, Ti = 0.06, Dy = 0.06, Y = 0.043, Yb = 0.02. Calculation were
922 carried out assuming: (a) a fractionating assemblage 0.60 plagioclase and 0.40 clinopyroxene and
923 that the composition of samples RF2 (Mg# = 63) and N10 (Mg# = 37) represent those of the most

924 primitive and most evolved basalt, respectively; (b) a fractionating assemblage 0.50 plagioclase and
925 0.50 clinopyroxene and that the compositions of samples ROS10 (Mg# = 65) and ROS6 (Mg# = 45)
926 represent those of the most primitive and most evolved basalt, respectively. *F* is the fraction of
927 remaining liquid (see text for further details).
928
929 **Fig. 11** Whole-rock basalt variation of CaO/Al_2O_3 vs. Ce_N/Sm_N
930
931 **Fig. 12** Variation of Zr_N/Y_N versus Ce_N/Sm_N in the clinopyroxenes. Literature data for (i)
932 clinopyroxene from plagioclase-rich peridotites (Rampone et al. 1997; Sanfilippo and Tribuzio
933 2011; Sanfilippo et al. 2014), olivine-rich troctolites (Borghini and Rampone 2007; Renna and
934 Tribuzio 2011) and gabbros (Rampone et al. 1997; Tribuzio et al. 1999; Sanfilippo and Tribuzio
935 2011; Tribuzio et al. 2014; Sanfilippo et al. 2015a) from the Jurassic Alpine-Apennine ophiolites
936 are also plotted.
937

Figure 1

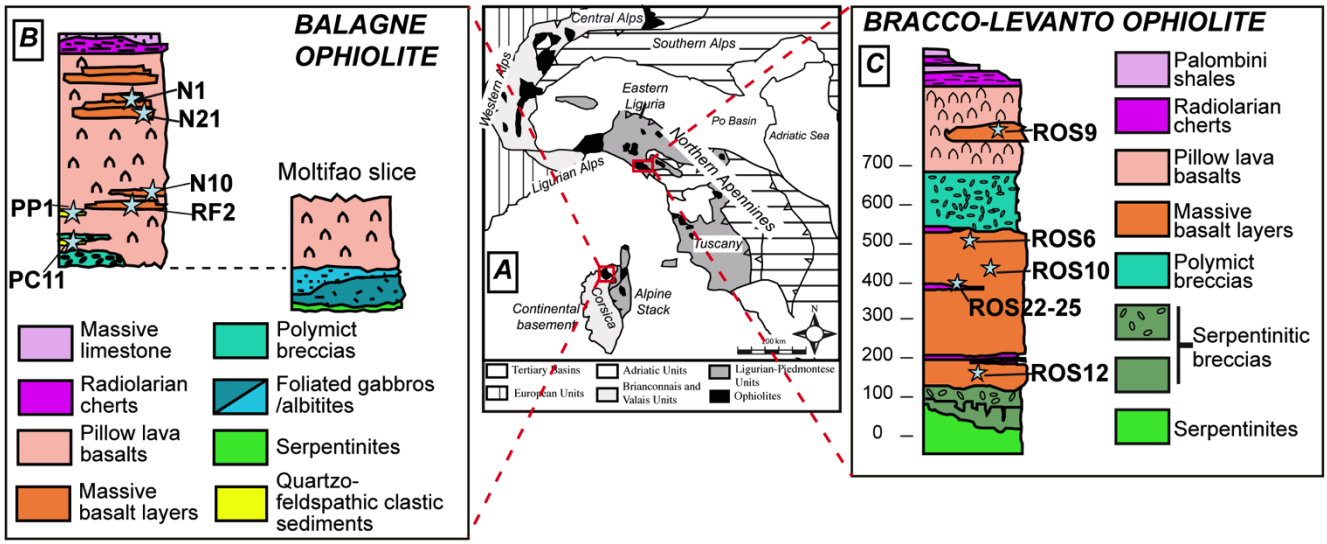
B
BALAGNE OPHIOLITE
N1
N21
N10
RF2
PP1
PC11
Moltifao slice
Massive limestone
Radiolarian cherts
Pillow lava basalts
Massive basalt layers
Polymict breccias
Foliated gabbros /albitites
Serpentinites
Quartzo-feldspathic clastic sediments
A
Central Alps
Southern Alps
Western Alps
Eastern Liguria
Po Basin
Adriatic Sea
Ligurian Alps
Northern Apennines
Tuscany
Alpine Stack
Continental basement
Corsica
Tertiary Basins
European Units
Adriatic Units
Brianconnais and Valais Units
Ligurian-Piedmontese Units
Ophiolites
C
BRACCO-LEVANTO OPHIOLITE
ROS9
ROS6
ROS10
ROS22-25
ROS12
700
600
500
400
300
200
100
0
Palombini shales
Radiolarian cherts
Pillow lava basalts
Massive basalt layers
Polymict breccias
Serpentinitic breccias
Serpentinites

Figure 2

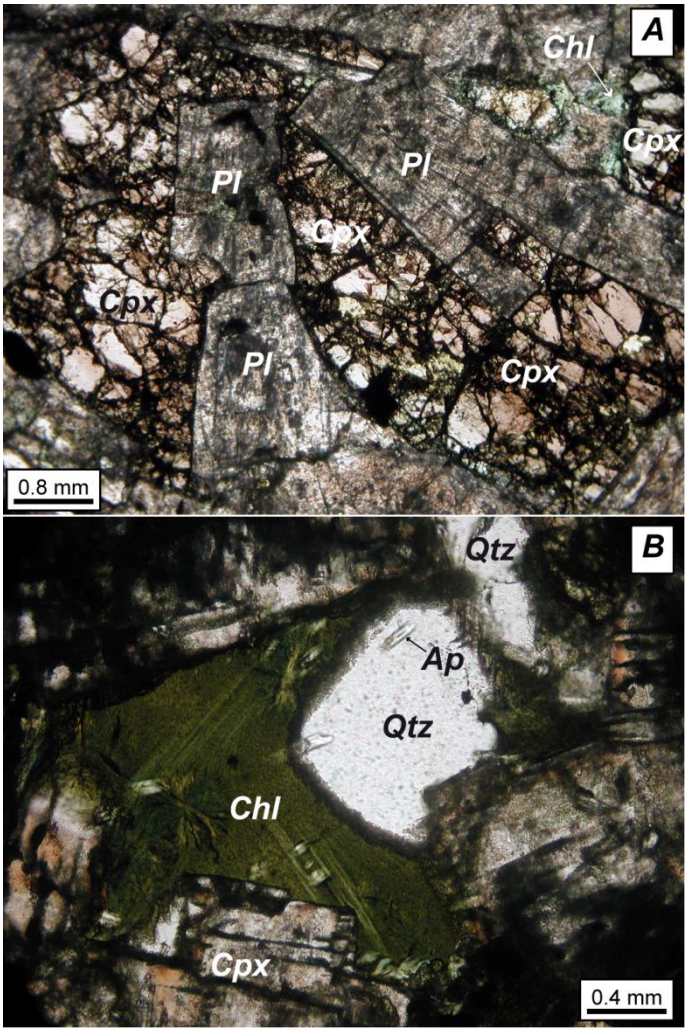

Figure 3

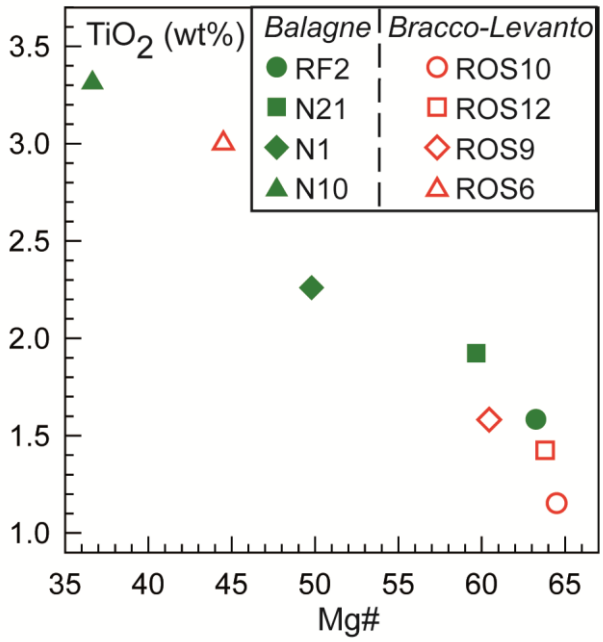
TiO2 (wt%)
Balagne
RF2
N21
N1
N10
Bracco-Levanto
ROS10
ROS12
ROS9
ROS6
3.5
3.0
2.5
2.0
1.5
1.0
35
40
45
50
55
60
65
Mg#

Figure 4

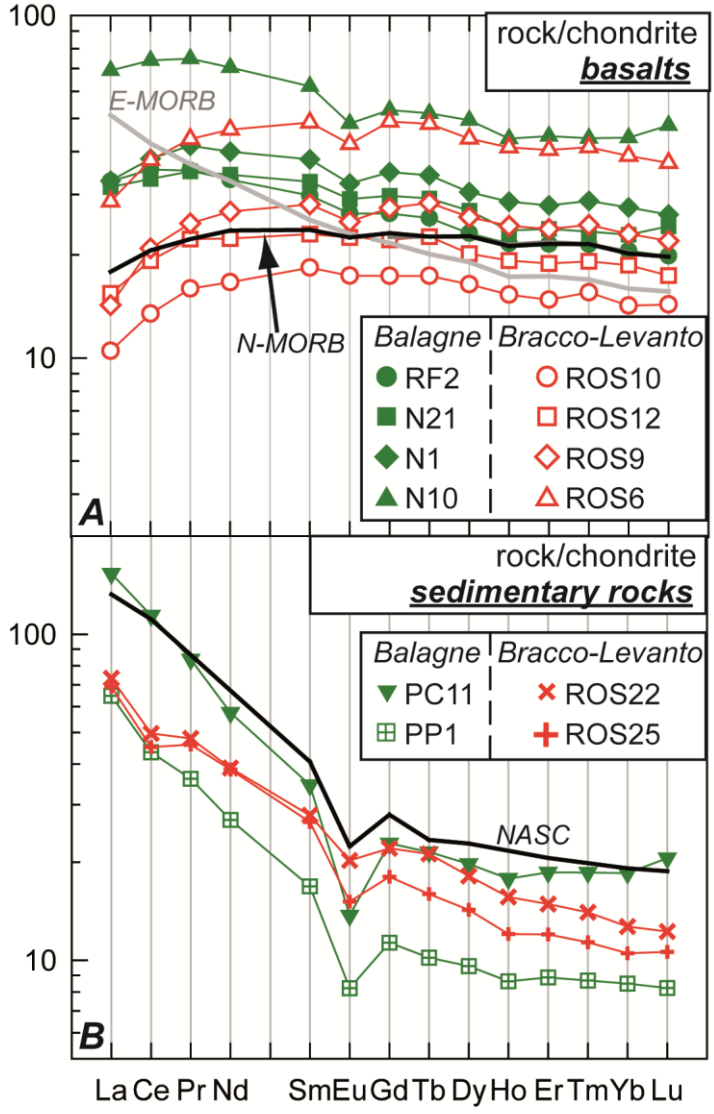

Figure 5

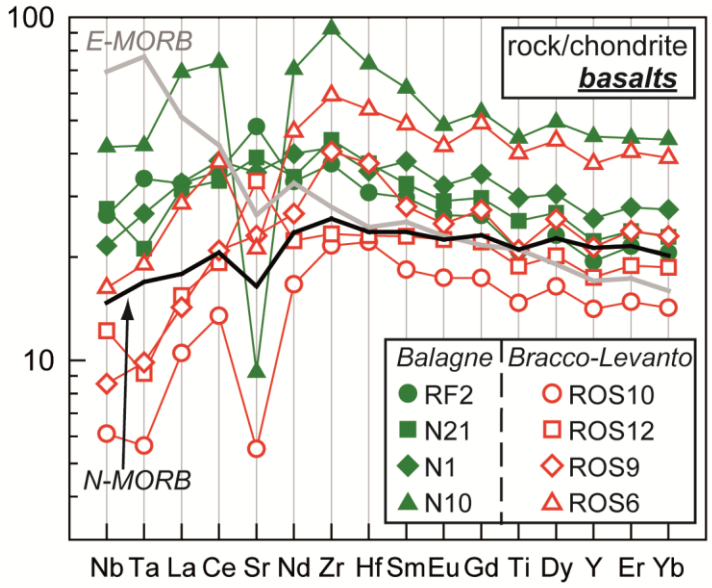
100
10
E-MORB
N-MORB
rock/chondrite
basalts
Balagne
Bracco-Levanto
RF2
N21
N1
N10
ROS10
ROS12
ROS9
ROS6
Nb Ta La Ce Sr Nd Zr Hf Sm Eu Gd Ti Dy Y Er Yb

Figure 6

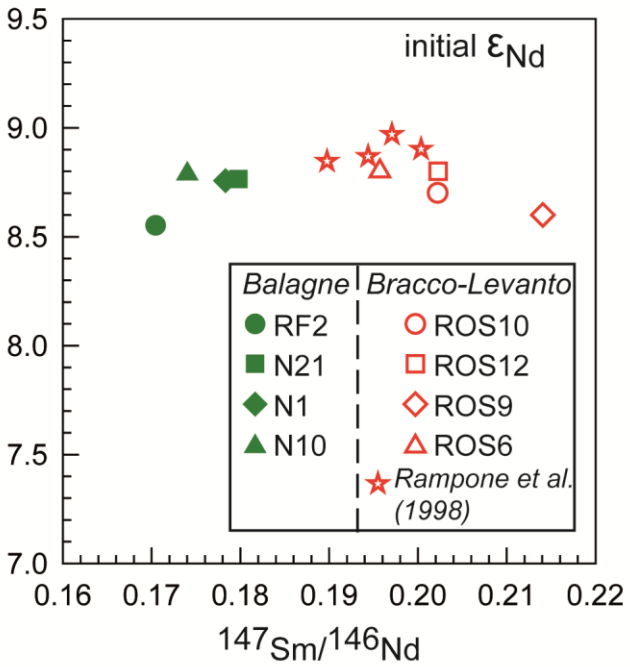

Figure 7

Click here to download Figure fig07_R1.ppt

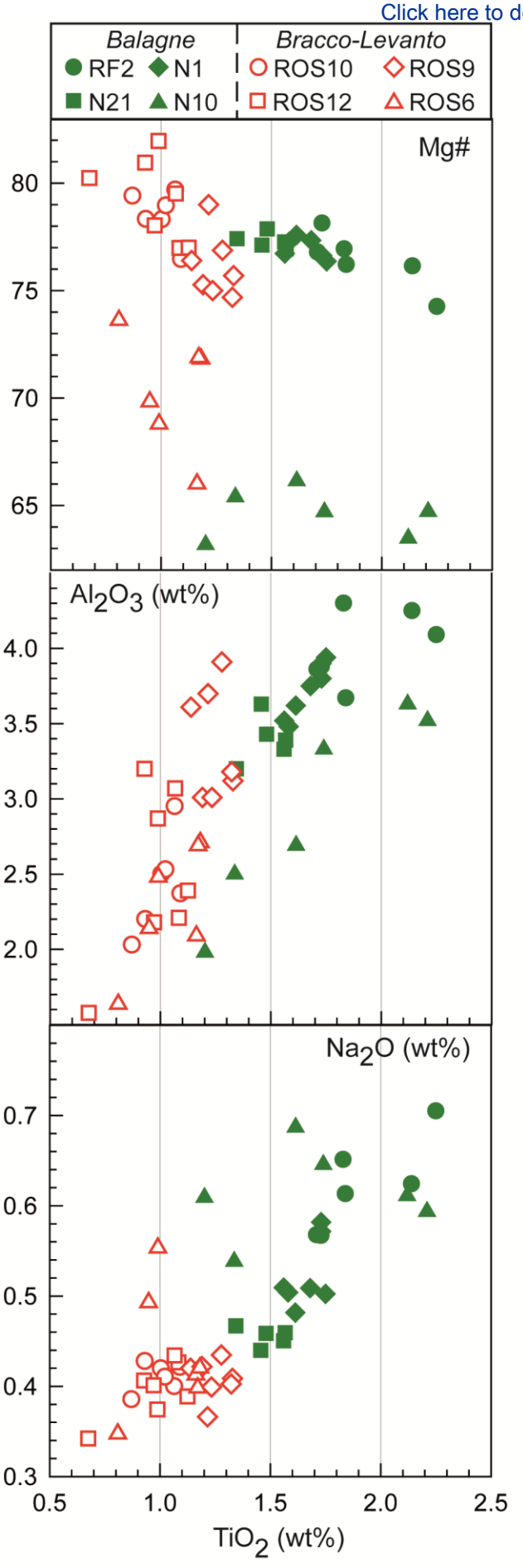

Figure 7

Figure 8

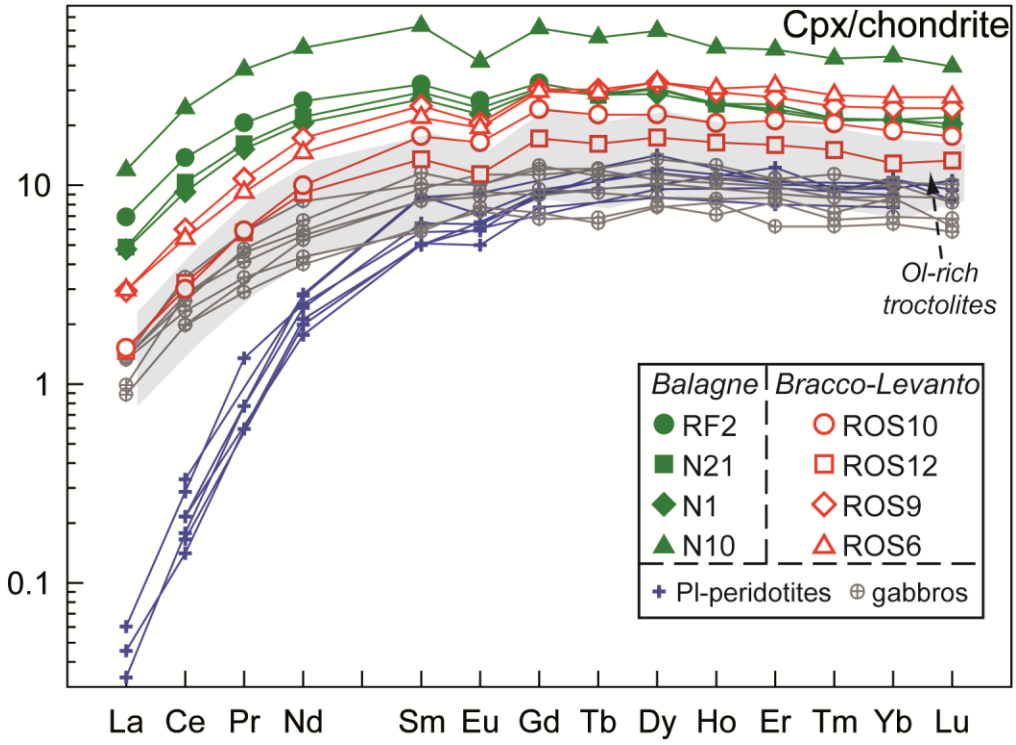

Figure 9

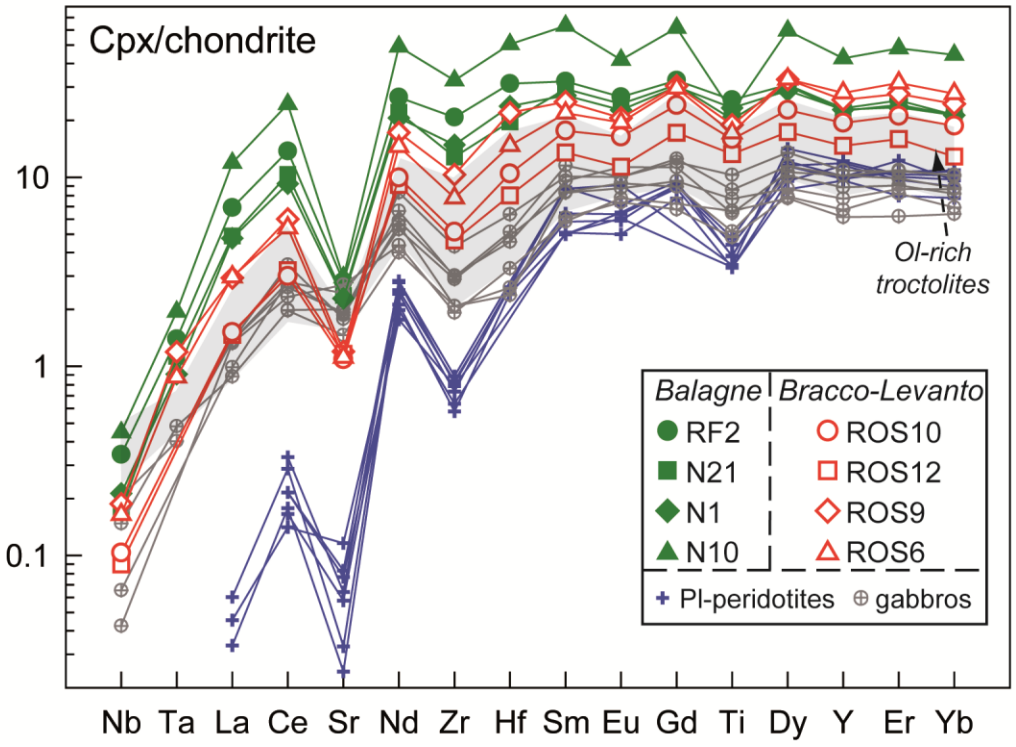

Figure 10

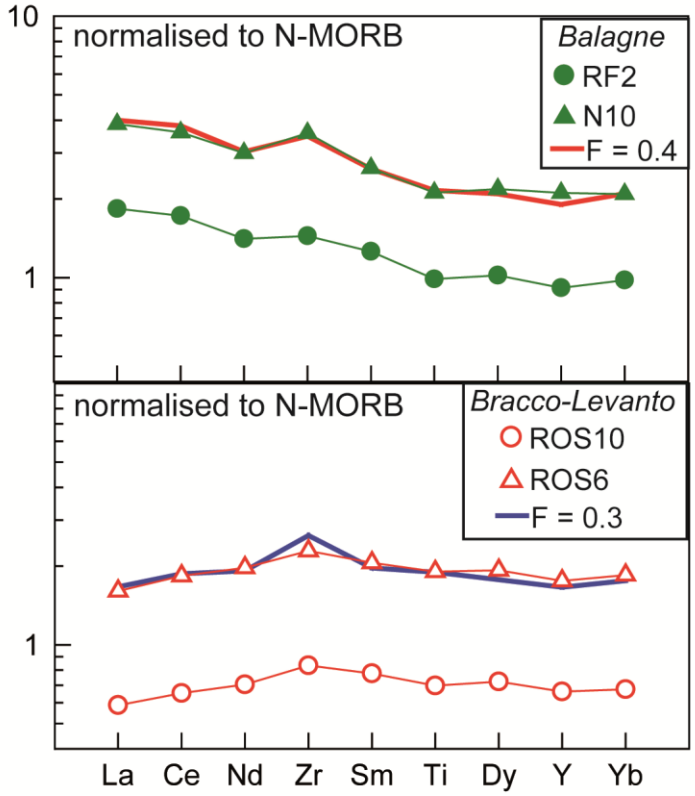

Figure 11

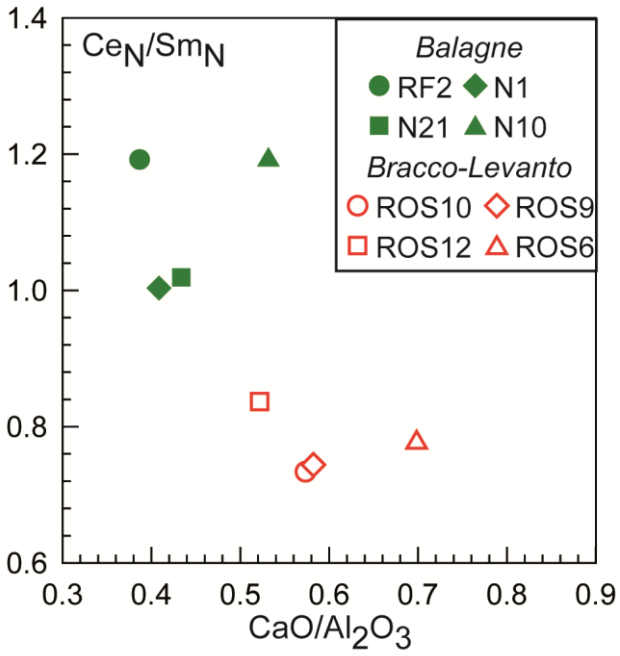

Figure 12

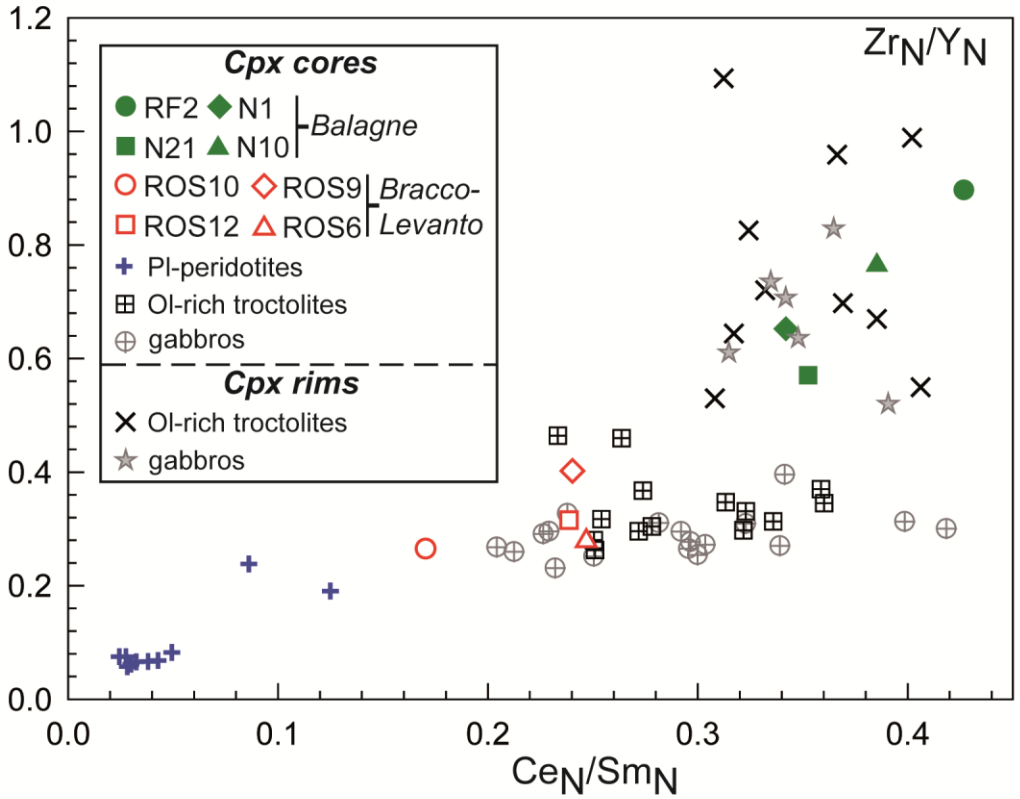

Table 1
Modal composition (vol. %) and petrographic features of the selected basalts, obtained by visual estimates.

ophiolite	Localization	Sample	locality	Pl		Cpx		Fe-Ti oxides		Qtz		Ap	Pl secondary transformation	Cpx secondary transformation
				vol%	grain size (mm)	vol%	grain size (mm)	vol%	grain size (mm)	vol%	grain size (mm)			
Balagne	Corsica	N1	Rio Casapola	60	0.8-4.0	35	0.3-2.0	5	0.2-0.6	—	—	tr	+++	++
Balagne	Corsica	N21	Rio Casapola	55	1.0-3.0	40	0.8-3.5	5	0.2-0.9	—	—	tr	+++	++
Balagne	Corsica	N10	Piantella	60	0.1-0.5	40	0.8-3.0	tr	0.2-0.6	—	—	tr	+++	++
Balagne	Corsica	RF2	Rio Forci	60	0.6-4.0	40	0.6-3.0	tr	0.3-1.5	—	—	tr	+++	+
Bracco-Levanto (Internal Ligurian units)	Northern Apennine	ROS6	Rossola	55	1.5-4.0	30	1.0-4.0	5	<0.8	5	0.2-0.8	tr	+++	++
Bracco-Levanto (Internal Ligurian units)	Northern Apennine	ROS9	Framura	55	1.0-5.0	45	0.5-2.0	tr	<0.2	—	—	tr	+++	++
Bracco-Levanto (Internal Ligurian units)	Northern Apennine	ROS10	Rossola	50	1.0-3.0	45	0.7-2.5	tr	<0.6	5	0.6-1.5	tr	+++	++
Bracco-Levanto (Internal Ligurian units)	Northern Apennine	ROS12	Rossola	60	0.5-3.5	40	1.0-3.0	tr	0.2-0.7	—	—	tr	+++	++

tr, < 4%; —, mineral not present in the rock

Extent of secondary transformation of plagioclase and clinopyroxene: +, ≤ 30%; ++, 30-90%; +++, ≥ 90%.

Mineral abbreviations after Kretz (1983).

Table 2
Whole-rock major and trace element compositions of selected samples

Sample	RF2	N21	N1	N10	ROS10	ROS12	ROS9	ROS6	PC11	PP1	ROS22	ROS25
rock-type	basalt	basalt	basalt	basalt	basalt	basalt	basalt	basalt	quartz-rich breccia	quartzitic sandstone	rad	rad
ophiolite	Balagne	Balagne	Balagne	Balagne	Br-Lev (IL)	Br-Lev (IL)	Br-Lev (IL)	Br-Lev (IL)	Balagne	Balagne	Br-Lev (IL)	Br-Lev (IL)
Major elements (wt%)												
SiO_2	51.3	49.5	50.1	49.9	46.9	48.1	48.9	47.7	71.1	54.9	76.3	73.2
TiO_2	1.51	1.85	2.16	3.23	1.07	1.37	1.53	2.91	0.24	0.17	0.17	0.17
Al_2O_3	16.4	15.0	15.7	13.4	16.5	17.3	15.3	12.8	13.6	4.97	4.62	4.60
$Fe_2O_3^{tot}$	7.40	10.1	9.67	13.6	8.57	8.34	9.54	14.6	2.89	0.95	9.86	9.77
MnO	0.17	0.16	0.19	0.23	0.11	0.15	0.17	0.21	0.06	0.05	0.15	0.36
MgO	6.43	7.55	4.84	3.97	7.86	7.42	7.36	5.92	0.69	1.06	4.35	4.96
CaO	6.36	6.52	6.42	7.14	9.47	9.01	8.92	8.91	1.19	20.1	0.50	1.57
Na_2O	5.55	4.20	4.95	5.39	2.14	4.00	3.88	3.62	3.08	1.09	0.12	0.13
K_2O	0.12	1.11	1.32	0.07	0.03	0.15	0.60	0.12	4.56	1.02	0.22	0.26
P_2O_5	0.27	0.27	0.30	0.57	0.10	0.15	0.21	0.35	0.07	0.04	0.13	0.15
L.O.I	3.08	3.30	2.75	2.44	5.78	3.96	3.58	2.87	1.99	16.2	2.99	2.69
CO_2	—	—	—	—	—	—	—	—	—	15.2	—	—
Total	98.6	99.6	98.4	100.0	98.5	99.9	100.0	100.0	99.5	100.5	99.4	97.9
Mg#	63.3	59.7	49.8	36.6	64.5	63.8	60.4	44.5	32.1	68.9	46.6	50.1
CaO/Al_2O_3	0.39	0.43	0.41	0.53	0.57	0.52	0.58	0.70	—	—	—	—
FeO^{tot}/MgO	1.04	1.20	1.80	3.08	0.98	1.01	1.17	2.22	—	—	—	—
Trace elements (ppm)												
V	184	240	255	351	138	220	264	375	17	16	92	103
Cr	120	130	40	<20	140	150	220	< 20	<20	<20	330	360
Sc	22	32	29	29	20	27	33	37	5	3	8	8
Co	27	39	25	34	32	32	36	38	3	<1	56	55
Ni	60	100	<20	<20	150	100	110	< 20	<20	<20	285	320
Cu	720	50	<10	20	50	50	50	40	<10	<10	40	70
Zn	<30	80	<30	120	40	< 30	50	110	40	<30	55	70
Ga	14	15	16	23	14	14	15	19	14	5	7	6
Sn	1	<1	1	4	1	< 1	2	3	3	2	1.0	< 1
Rb	<1	9.0	11.0	<1	< 1	4	12	1	196	34	7	7
Sr	374	304	275	72	43	260	180	165	92	111	50.5	52
Ba	17	32	33	13	6	8	35	10	528	101	31.0	39
Zr	147	173	164	364	85	92	160	233	140	97.0	35.5	35
Nb	6.50	6.80	5.30	10.3	1.50	3.00	2.10	4.00	11	3.7	2.6	1.8
Y	30.3	34.7	40.4	70.0	22	27.2	33.3	58.3	27.8	16.4	26.7	19.7
Hf	3.20	3.90	3.70	7.60	2.30	2.40	3.90	5.60	4.30	2.40	0.80	0.4
Ta	0.48	0.30	0.38	0.60	0.08	0.13	0.14	0.27	1.25	0.46	0.16	0.02
Pb	<5	<5	<5	<5	< 5	< 5	< 5	< 5	11	12	8	19
Th	0.40	0.30	0.39	0.78	0.17	0.24	0.16	0.32	15.3	5.87	2.69	2.56
U	0.17	0.11	0.20	0.28	0.08	0.09	0.09	0.33	3.29	2.10	0.50	0.54
La	7.69	7.40	7.72	16.20	2.46	3.62	3.35	6.72	36.0	15.2	17.2	16.2
Ce	21.4	20.1	23.0	44.6	8.12	11.6	12.6	22.8	68.9	26.2	30.0	27.2
Pr	3.14	3.12	3.71	6.66	1.42	1.98	2.20	3.88	7.47	3.21	4.27	4.09
Nd	15.0	15.5	18.1	31.9	7.52	10.1	12.1	21.0	26.0	12.2	17.6	17.4
Sm	4.38	4.81	5.59	9.13	2.70	3.38	4.13	7.16	5.08	2.48	4.10	3.91
Eu	1.48	1.63	1.81	2.71	0.97	1.26	1.40	2.36	0.77	0.46	1.14	0.85
Gd	5.19	5.85	6.85	10.40	3.41	4.35	5.39	9.63	4.49	2.23	4.34	3.55
Tb	0.93	1.06	1.24	1.88	0.63	0.82	1.03	1.75	0.78	0.37	0.77	0.58
Dy	5.61	6.53	7.40	12.00	3.98	4.89	6.26	10.6	4.80	2.33	4.41	3.47
Ho	1.20	1.31	1.59	2.43	0.85	1.07	1.35	2.29	0.99	0.48	0.87	0.67
Er	3.41	3.78	4.43	7.06	2.35	3.00	3.78	6.43	2.96	1.41	2.37	1.91
Tm	0.52	0.57	0.70	1.06	0.38	0.46	0.59	1.00	0.45	0.21	0.34	0.28
Yb	3.34	3.72	4.47	7.14	2.31	3.03	3.74	6.32	3.01	1.38	2.07	1.71
Lu	0.48	0.59	0.64	1.16	0.35	0.42	0.53	0.90	0.50	0.20	0.30	0.26
Ce_N/Sm_N	1.19	1.02	1.00	1.19	0.73	0.84	0.74	0.78	4.44	3.84	2.63	2.60
Gd_N/Yb_N	1.28	1.30	1.27	1.20	1.22	1.19	1.19	1.26	1.23	1.34	1.74	1.72
Eu/Eu*	0.94	0.93	0.89	0.84	0.97	1.00	0.90	0.86	0.49	0.59	0.82	0.69
Nb_N/Y_N	1.36	1.24	0.83	0.93	0.43	0.70	0.40	0.44	—	—	—	—
Ta_N/Y_N	1.74	0.95	1.03	0.94	0.40	0.53	0.46	0.51	—	—	—	—
Zr_N/Y_N	1.92	1.97	1.61	2.06	1.53	1.34	1.90	1.58	—	—	—	—
Hf_N/Y_N	1.58	1.69	1.37	1.63	1.57	1.32	1.76	1.44	—	—	—	—
$(Sm/Yb)_{DM}$	1.79	1.76	1.70	1.74	1.59	1.52	1.50	1.54	—	—	—	—

rad, radiolarian chert; Br-Lev (IL), Bracco-Levanto (Internal Ligurian units)

L.O.I. loss on ignition. Mg# = 100 × molar $Mg/(Mg+Fe^{2+}_{tot})$

—, not determined; $(Sm/Yb)_{DM}$, Sm/Yb normalized to depleted mantle ratios (see Hirschmann and Stolper, 1996)

Table 3
Nd isotope compositions of selected samples

Sample	rock-type	ophiolite	$^{143}Nd/^{144}Nd \pm 2$ s.e.	Sm	Nd	$^{147}Sm/^{144}Nd$	$^{143}Nd/^{144}Nd_{(164\ Ma)}$	ε_{Nd}	$\varepsilon_{Nd\ (164Ma)}$
RF2	basalt	Balagne	0.513048 ± 4	3.9601	14.157	0.1705	0.51287 ± 4	+8.0	+8.6 ± 0.1
N10	basalt	Balagne	0.513064 ± 4	8.6910	30.435	0.1740	0.51288 ± 4	+8.3	+8.8 ± 0.1
N1	basalt	Balagne	0.513067 ± 4	5.1997	17.771	0.1783	0.51288 ± 4	+8.4	+8.8 ± 0.1
N21	basalt	Balagne	0.513069 ± 4	4.5068	15.277	0.1798	0.51288 ± 4	+8.4	+8.8 ± 0.1
PC11	quartzo-feldspathic breccia	Balagne	0.512269 ± 4	4.5772	23.652	0.1179	0.51214 ± 4	-7.2	-5.5 ± 0.1
			$^{143}Nd/^{144}Nd \pm 2$ s.e.	Sm	Nd	$^{147}Sm/^{144}Nd$	$^{143}Nd/^{144}Nd_{(161Ma)}$	ε_{Nd}	$\varepsilon_{Nd\ (161Ma)}$
ROS6	basalt	Bracco-Levanto	0.513086 ± 4	3.1666	9.8610	0.1957	0.51288 ± 4	+8.7	+8.8 ± 0.1
ROS9	basalt	Bracco-Levanto	0.513095 ± 4	2.5091	7.1434	0.2141	0.51287 ± 4	+8.9	+8.6 ± 0.1
ROS10	basalt	Bracco-Levanto	0.513090 ± 4	7.2307	21.7887	0.2022	0.51288 ± 4	+8.8	+8.7 ± 0.1
ROS12	basalt	Bracco-Levanto	0.513094 ± 4	3.9663	11.9496	0.2023	0.51288 ± 4	+8.9	+8.8 ± 0.1
ROS23	radiolarian chert	Bracco-Levanto	0.512315 ± 4	3.6082	15.239	0.1443	0.51216 ± 4	-6.3	-5.2 ± 0.1

2 s.e. is the uncertainty on measured $^{143}Nd/^{144}Nd$ (internal precision).

The assessment of errors on calculated $^{143}Nd/^{144}Nd$ ratios and corresponding ε values was done using the error propagation equation reported in Blichert-Toft et al. (1995)

Table 4
Representative major element clinopyroxene compositions (wt%)

Sample	RF2	N21	N1	N10	ROS10	ROS12	ROS9	ROS6
ophiolite	Balagne	Balagne	Balagne	Balagne	Br-Lev (IL)	Br-Lev (IL)	Br-Lev (IL)	Br-Lev (IL)
SiO_2	50.3	50.3	50.3	49.5	51.2	52.1	51.2	51.5
TiO_2	1.84	1.84	1.68	1.74	1.00	0.97	1.14	0.95
Al_2O_3	3.67	3.67	3.75	3.33	2.50	2.18	3.61	2.14
Cr_2O_3	0.12	0.12	0.09	0.04	0.25	0.10	0.35	0.05
FeO	7.91	7.9	7.82	11.41	7.67	7.97	8.30	10.3
MnO	0.21	0.21	0.23	0.29	0.21	0.19	0.20	0.36
NiO	<0.02	<0.02	0.02	<0.02	<0.02	0.06	0.05	<0.02
MgO	14.2	14.2	15.0	11.7	15.5	15.9	15.1	13.3
CaO	21.7	21.7	20.9	20.7	19.2	20.1	19.9	20.7
Na_2O	0.61	0.61	0.51	0.65	0.42	0.40	0.42	0.49
K_2O	0.01	0.01	0.01	<0.01	<0.01	<0.01	<0.01	<0.01
Sum	100.5	100.5	100.3	99.3	98.0	100.0	100.2	99.8
Mg#	76.2	76.2	77.3	64.7	78.3	78.0	76.4	69.8

Br-Lev (IL), Bracco-Levanto (Internal Ligurian units)

Mg#, [100 × Mg/(Mg+Fe^{2+}_{tot}), in atoms per formula unit]

Table 5
Trace element compositions of the clinopyroxenes (ppm)

Sample	RF2	N21	N1	N10	ROS10	ROS12	ROS9	ROS6
ophiolite	Balagne	Balagne	Balagne	Balagne	Br-Lev (IL)	Br-Lev (IL)	Br-Lev (IL)	Br-Lev (IL)
V	576	512	572	629	369	347	512	484
Cr	1,410	578	662	11	1,200	1,260	1,600	155
Sc	152	132	163	136	128	109	147	140
Ti	11,200	8,840	10,100	9,630	6,930	5,780	8,260	7,480
Rb	0.07	0.06	<0.04	<0.04	<0.04	0.05	0.05	0.08
Sr	21.9	18.5	17.9	23.1	8.49	9.09	9.34	8.71
Ba	0.21	0.28	0.13	0.20	0.06	0.10	0.24	0.17
Zr	81.8	50.5	58.5	128	20.2	18.3	40.7	30.7
Nb	0.08	0.04	0.05	0.11	0.03	0.02	0.05	0.04
Y	36.1	35.0	35.5	66.4	30.3	22.9	40.0	43.6
Hf	3.25	2.05	2.47	5.25	1.09	0.83	2.28	1.53
Ta	0.02	0.02	0.01	0.03	<0.01	<0.01	0.02	0.01
La	1.62	1.15	1.12	2.79	0.36	0.34	0.69	0.70
Ce	8.29	6.25	5.58	14.7	1.81	1.95	3.63	3.25
Pr	1.83	1.44	1.35	3.40	0.53	0.52	0.96	0.82
Nd	12.0	9.99	9.32	22.2	4.51	4.13	7.81	6.58
Sm	4.73	4.32	3.98	9.31	2.59	1.99	3.69	3.22
Eu	1.49	1.37	1.27	2.34	0.92	0.64	1.15	1.09
Gd	6.40	6.06	5.92	12.1	4.73	3.38	5.98	5.82
Tb	1.05	1.03	1.03	2.01	0.82	0.59	1.10	1.06
Dy	7.48	7.38	6.98	14.5	5.50	4.22	7.99	8.02
Ho	1.43	1.42	1.42	2.73	1.14	0.91	1.64	1.70
Er	4.05	3.84	3.72	7.65	3.35	2.53	4.39	5.01
Tm	0.52	0.52	0.51	1.05	0.49	0.36	0.60	0.69
Yb	3.47	3.47	3.46	7.22	3.05	2.09	3.97	4.50
Lu	0.47	0.53	0.50	0.96	0.43	0.32	0.59	0.67
La_N/Sm_N	0.43	0.35	0.34	0.39	0.17	0.24	0.24	0.25
Eu/Eu*	0.82	0.81	0.79	0.67	0.80	0.75	0.75	0.77
Sr/Sr*	0.15	0.16	0.17	0.09	0.20	0.21	0.12	0.13
Gd_N/Yb_N	1.53	1.44	1.42	1.39	1.28	1.34	1.24	1.07
Nb_N/Y_N	0.01	0.01	0.01	0.01	0.01	0.01	0.01	0.01
Ta_N/Y_N	0.06	0.05	0.04	0.05	–	–	0.05	0.03
Hf_N/Y_N	1.35	0.88	1.04	1.19	0.54	0.55	0.85	0.53
Zr_N/Y_N	0.90	0.57	0.65	0.76	0.26	0.32	0.40	0.28

Br-Lev (IL), Bracco-Levanto (Internal Ligurian units)

$Eu/Eu^* = Eu_N/(Sm_N \times Gd_N)^{1/2}$; $Sr/Sr^* = Sr_N/(Ce_N \times Nd_N)^{1/2}$

Click here to access/download

Electronic supplementary material

QC_WR analyses (SM).xlsx